

Final Draft
of the original manuscript:

Schloffer, M.; Iqbal, F.; Gabrisch, H.; Schwaighofer, E.; Schimansky, F.-P.;
Mayer, S.; Stark, A.; Lippmann, T.; Goeken, M.; Pyczak, F.; Clemens, H.:
**Microstructure development and hardness of a powder
metallurgical multi phase γ -TiAl based alloy**
In: Intermetallics (2011) Elsevier

DOI: 10.1016/j.intermet.2011.11.015

Microstructure development and hardness of a powder metallurgical multi phase γ -TiAl based alloy

Martin Schloffer ^{a*}, Farasat Iqbal ^b, Heike Gabrisch ^c, Emanuel Schwaighofer ^a, Frank-Peter Schimansky ^c, Svea Mayer ^a, Andreas Stark ^c, Thomas Lippmann ^c, Mathias Göken ^b, Florian Pyczak ^c, Helmut Clemens ^a

^a Department of Physical Metallurgy and Materials Testing, Montanuniversität Leoben, A-8700 Leoben, Austria

^b Institute of General Materials Properties, WWI Department of Materials Science and Engineering, University of Erlangen-Nuremberg, D-91058 Erlangen, Germany

^c Institute of Materials Research, Helmholtz-Zentrum Geesthacht, D-21502 Geesthacht, Germany

Keywords: A. titanium aluminides; B. grain growth, phase transformation; C. powder metallurgy; D. microstructure

ABSTRACT

A β -solidifying TiAl alloy with a nominal composition of Ti-43.5Al-4Nb-1Mo-0.1B (in at.%), termed TNM™ alloy, was produced by a powder metallurgical approach. After hot-isostatic pressing the microstructure is comprised of fine equiaxed γ -TiAl, α_2 -Ti₃Al and β_0 -TiAl grains. By means of two-step heat-treatments different fine grained nearly lamellar microstructures were adjusted. The evolution of the microstructure after each individual heat-treatment step was examined by light-optical, scanning and transmission electron microscopy as well as by conventional X-ray and in-situ high-energy X-ray diffraction. The experimentally evaluated phase fractions as a function of temperature were compared with the results of a thermodynamical calculation using a commercial TiAl database. Nano-hardness measurements have been conducted on the three constituting phases α_2 , γ and β_0 after hot-isostatic pressing, whereas the hardness modification during heat-treatment was studied by macro-hardness measurements. A nano-hardness for the β_0 phase is reported for the first time.

1. Introduction

The continuous demand for weight reduction and higher engine efficiencies in automotive, aerospace and energy industries pushes the currently applied materials towards their limits. Therefore, these industries have a strong need for the development of novel lightweight materials which can withstand temperatures up to 800°C, while maintaining acceptable mechanical properties. Intermetallic γ -TiAl based alloys are among the most promising candidates, which possess these required thermal and mechanical properties [1]. In 1999 the first commercial application of γ -TiAl based alloys was announced. Mitsubishi has implemented TiAl turbocharger wheels in their Lancer 6 sports car [2]. In 2002, the commercial production of wrought high-performance γ -TiAl valves for racing car application has started. Recently, an US aero-engine manufacturer announced the initiation of investment cast γ -TiAl blades in the low-pressure turbine. Certification and flight tests with TiAl equipped engines have been conducted successfully and the begin of the regular service for passenger transport is expected soon [3]. Meanwhile also other major aero-engine manufactures have announced the use of TiAl in the near future. It has been shown that cast TiAl alloys based on Ti-(41-45)Al with additions of Nb, Mo and B solidify via the disordered body-centred cubic (bcc) β -Ti(Al) phase, exhibiting a very fine grained and texture-free microstructure with modest micro-segregations [4,5,6], whereas

peritectic alloys (i.e. solidification via the disordered hexagonal close-packed (hcp) α -Ti(Al) phase) show anisotropic microstructures as well as significant texture and segregation [7].

One well known example of these β -solidifying alloys is the alloy named TNMTM. The name stems from the fact that Nb and Mo represent the most relevant alloying elements in TNMTM. In TNMTM alloys the volume fraction of the β -phase can be controlled by choosing appropriate forging and/or heat treatment temperatures [5]. The disordered bcc β -lattice provides a sufficient number of independent slip systems and therefore acts as a deformation accommodating phase at elevated temperatures. In a previous study it has been shown that these alloys exhibit an improved deformability at elevated temperatures, where, for example, hot-working processes such as rolling and forging are performed [8]. However, at service temperature, which is in the range of 700°C to 800°C, the presence of a creep resistant lamellar microstructure is preferred, consisting of lamellar γ -TiAl/ α_2 -Ti₃Al-colonies with a size smaller than 100 μm . The γ -TiAl phase exhibits a tetragonal L1₀ structure, whereas the ordered hexagonal α_2 -phase crystallizes with DO₁₉ structure. The volume fraction of globular β_0 -phase, which shows an ordered B2 structure at service temperature, should be small or negligible to prevent deterioration of the creep properties [9]. The same applies for the presence of small globular γ -grains, which tend to arrange at the boundaries of α_2/γ -colonies. For the TNMTM alloy, which spans a composition range of Ti-(42-44)Al-(3-5Nb)-(0.1-2)Mo-(0.1-1)B (all compositions are given in atomic percent (at.%), unless stated otherwise), it was demonstrated that the β_0 volume fraction can effectively be reduced by subsequent two-step heat-treatments, leading to balanced mechanical properties, i.e. good creep strength and sufficient plastic fracture strain at room temperature [8].

After the first heat-treatment in the temperature range of the ($\alpha + \beta$) or ($\alpha + \beta + \gamma$) phase field region rapid cooling results in a microstructure consisting of a small volume fraction of globular β_0 -grains or β_0 - and γ -grains as well as larger supersaturated α_2 -grains depending on the selected annealing temperature. The second heat-treatment step, which consists of an ageing treatment in the ($\alpha_2 + \beta_0 + \gamma$) phase field region, has a strong effect on the mechanical properties. Microstructural investigations revealed that the observed increase in yield strength and in creep resistance can be attributed to the formation of fine γ -lamellae within the supersaturated α_2 -grains, meaning that these properties are strongly correlated to the smallest dimension in the microstructure, i.e. the mean interface spacing [10] or, more precisely, the average lamellar widths [11]. The formation of γ -lamellae is accompanied by a significant increase in the γ -phase fraction. Furthermore, as the temperature of the second heat-treatment step increases from 850°C up to 900°C, the microstructure shows a higher fraction of colonies transformed by a cellular reaction [12]. The material's strength and hardness were shown to be primarily connected to the lamellar spacing within the colonies, where the strength increases with decreasing lamellar spacing [5,8].

In this study, the microstructural development in an alloy of the TNM family that was produced by powder metallurgy (PM) was investigated for the first time. The exact composition of the alloy is Ti-43.9Al-4.0Nb-0.95Mo-0.1B. When this alloy is processed above the γ -solvus temperature ($T_{\gamma\text{solv}}$) the resulting nearly lamellar (NL) microstructure contains β_0 -phase between the lamellar α_2/γ -colonies. In the following this particular type of microstructure is called NL+ β . Consequently, microstructures which are heat-treated below

$T_{\gamma_{\text{soliv}}}$, but above the eutectoid temperature (T_{eut}), are termed NL+ γ because they exhibit a dominant volume fraction of globular γ (γ_g), which is primarily situated on colony boundaries and triple points. Additionally, a small volume fraction of β_o -phase is present, depending on the specific annealing temperature. From a previous study it is evident that the plastic fracture strain below the brittle-to-ductile temperature is strongly related to the homogeneity of the microstructure, i.e. the microstructural quality [13]. It was shown that a homogeneous microstructure with a narrow grain size distribution possesses a significantly higher plastic fracture strain at room temperature than a fine-grained microstructure with embedded coarse grains.

The aim of this study was to design two-step heat-treatments for the controlled adjustment of NL microstructures exhibiting on the one hand a high microstructural quality in terms of colony size distribution and on the other hand showing an even arrangement of the phases within the microstructure. As mentioned above, the first heat-treatment step consists of annealing in the ($\alpha + \beta$) or ($\alpha + \beta + \gamma$) phase field region. The coarsening of the α -grains depends on temperature, time, and volume fraction of the present minority phases (β/γ or β). Especially the cooling rate after the first heat-treatment is crucial in order to provide supersaturated α_2 -grains from which the lamellar α_2/γ -colonies are generated during the second heat-treatment. The most important parameters of the second heat-treatment step, which is in fact an ageing treatment, are annealing temperature and holding time. A too high annealing temperature or a prolonged annealing time can trigger the onset of the cellular reaction, which partly consumes the lamellar colonies. More information on the cellular reaction in TNM™ alloys are given in ref. [12]. After every individual heat-treatment step the prevailing microstructure was analyzed by means of quantitative and qualitative metallography. In order to obtain a first impression on the material's strength macro-hardness measurements according to Vickers were conducted. In addition, nano-indentation was employed to study the hardness of the individual phases. The use of PM material is particularly advantageous compared with cast material because the processing route offers the possibility to achieve a starting material which exhibits a homogeneous fine-grained and almost segregation-free microstructure. In addition, hot-isostatically pressed (HIPed) PM-material shows a very weak texture [14]. More details on PM processing of γ -TiAl based alloys can be found in the review paper of Gerling et al. [14].

2. Material, experimental details and thermodynamic calculations

TNM™ PM material with a composition Ti-43.9Al-4.0Nb-0.95Mo-0.1B was produced by argon gas atomization using the Electrode Induction Melting Gas Atomization technique (EIGA) [14]. In this technique the pre-alloyed rod dips into a conical induction coil. Upon operation of the coil the tip of the rod is heated and melts. In the centre of a gas nozzle, the melt is atomized by argon gas. Powder with a particle size smaller than 180 μm in diameter was filled into cylindrical titanium cans with an inner diameter of 48.5 mm. Subsequently, the capsules were evacuated, sealed and HIPed at 1250°C for 2 h at 200 MPa, followed by furnace cooling. It should be noted that all processing steps involving the atomized powder are either done under argon atmosphere or under vacuum and that the powder did not experience any exposure to air, oxygen or nitrogen. For the subsequent heat-treatments, samples measuring approximately 5x5x5 mm³ and 10x10x10 mm³ as well as discs with \varnothing 44 mm x 20 mm were cut from the HIPed material. All heat-treatments were performed in a Carbolite furnace RHF 1600, where the temperature was controlled with thermocouples.

1 One type R thermocouple was located in the corner of the furnace, whereas a type S thermocouple was
2 positioned close to the surface of the sample. The latter one was used to control the temperature of the
3 sample. Before the samples were transferred to the heating chamber, the furnace was held at temperature
4 for at least 1 hour. During the sample holding time the recorded temperature changes were not larger than
5 $\pm 1^\circ\text{C}$. The subsequent water quenching (WQ) was performed in 17°C cold water, whereas for air cooling
6 (AC) the samples were put on a fireclay plate at room temperature. Furnace cooling (FC) was conducted in
7 the closed furnace by switching off the furnace till the samples cooled down to room temperature at a rate of
8 approximately 5 K/min. Up to 1265°C the holding time was 1 hour. For annealing above 1265°C , however,
9 the holding time was reduced to 9, 12 and 30 minutes, respectively, in order to study and to prevent
10 excessive grain coarsening. The holding time at 850°C and 900°C , which is the temperature range of the
11 second heat-treatment step, was 6 hours. The small samples with $5\times 5\times 5\text{ mm}^3$ were used to evaluate the
12 prevailing microstructural constituents in the temperature range of 1075°C to 1285°C . The larger samples
13 with approximately $10\times 10\times 10\text{ mm}^3$ were used to study the microstructure and phase fractions after annealing
14 between 1290°C and 1350°C for 9 minutes up to 30 minutes and subsequent cooling with different rates.
15 The cylindrical samples with $\text{Ø}44\text{ mm} \times 20\text{ mm}$ were used for Vickers hardness (HV10) measurements,
16 nano-indentation and two-step heat-treatments. For the heat-treatments of these specimens the following
17 parameters were selected: $1290^\circ\text{C}/12\text{ min}/\text{AC}$ (1st step) + $850^\circ\text{C}/6\text{ h}/\text{FC}$ (2nd step). The longer holding time at
18 the first heat-treatment step, 12 minutes compared to 9 minutes for the smaller specimens, was chosen to
19 obtain an identical α_2 -grain size. The second step of the heat-treatment was used to induce the formation of
20 γ -lamellae within the supersaturated α_2 -grains [8].
21
22
23
24
25
26
27
28
29

30 For subsequent conventional X-ray diffraction (XRD) and scanning electron microscopy (SEM) investigations
31 the samples were cut, ground and etched electrolytically [15]. For the XRD investigations a Bruker-AXS D8
32 Advance Diffractometer in Bragg-Brentano geometry was used with $\text{Cu-K}\alpha$ radiation. To evaluate the phase
33 fractions from the XRD patterns Rietveld analysis was performed with the commercial software package
34 TOPAS by Bruker AXS, Madison, USA. The SEM examinations were conducted on a Zeiss EVO 50 with a
35 LaB_6 cathode and a Zeiss CrossBeam 1540 with a Field Emission Gun (FEG). In order to analyse the
36 microstructural constituents and their grain size with light-optical microscope (LOM) the samples from heat-
37 treatments, conducted between 1240°C and 1285°C , were thermally etched at 900°C for 2 minutes to enable
38 the detection of grain boundaries. Additionally, the samples were colour-etched electrolytically using an Ence
39 and Margolin solution [16] as described in [15] and were examined with a LOM from Zeiss, Type Axio Imager
40 M1m. The fine lamellar structure cannot be analyzed by SEM with sufficient accuracy. Therefore,
41 transmission electron microscopy (TEM) was used on the sample that had experienced the following heat-
42 treatment: $1290^\circ\text{C}/12\text{min}/\text{AC} + 850^\circ\text{C}/6\text{ h}/\text{FC}$ (HT3, see Table 1). Specimens for TEM investigation were cut,
43 ground and polished and subsequently electrolytically thinned to electron transparency using an agent of
44 perchloric acid and butanol. The specimens were characterized in a Philips (now FEI) CM200 operating at
45 an acceleration voltage of 200 kV. All TEM-micrographs were recorded after tilting to γ - $\langle 110 \rangle$ zone axes
46 where the lamellae's are projected edge-on. For the evaluation of phase fractions and grain sizes for each
47 heat-treatment at least ten LOM images were analyzed in order to achieve good statistics. The results
48 derived from LOM images were then compared with the results obtained from three SEM images. The
49 contrast of the LOM and SEM images was optimized with Adobe[®] Photoshop[®] CS5. The evaluation of phase
50
51
52
53
54
55
56
57
58
59
60
61
62
63
64
65

1 fraction and grain size (LOM, SEM), as well as the measurement of distances between γ -lamellas (TEM) was
2 performed using the commercial software AnalySIS[®] from Olympus Soft Imaging System GmbH, Germany.

3 For the in-situ synchrotron experiments the high-energy X-ray diffraction (HEXRD) setups of the HZG
4 beamline HARWI II at DESY in Hamburg, Germany, were used [17,18,19]. Specimens with a diameter of
5 5 mm and a length of 15 mm were heated in a quenching and deformation dilatometer Bähr DIL 805 A/D
6 from Bähr-Thermoanalyse GmbH under Ar-atmosphere [20]. The temperature of the cylindrical samples was
7 controlled with a type B thermocouple. For the 0.5x0.5 mm² beam a mean energy of 104.7 keV was
8 adjusted. The samples were rapidly heated to 1000°C, held at that temperature for 10 min, and then
9 continuously heated at a rate of 2 K/min to 1350°C. A mar555 detector by Marresearch GmbH, Norderstedt,
10 Germany, was employed. The azimuthal integration of the acquired diffraction patterns was performed with
11 the software fit2D [21]. For Rietveld analysis the commercial software package TOPAS was used. More
12 details about the use of synchrotron radiation for the characterization of γ -TiAl based alloys are given in
13 references [17,22,23].

14
15
16
17
18
19
20
21 The macro-hardness according to Vickers was measured using an Emco-test M4C 025 G3M. The hardness
22 of the constituent phases as well as the reduced modulus were determined by nanoindentation employing a
23 Veeco Multimode AFM with built-in Triboscope from Hysitron Inc., USA. The samples were prepared by
24 grinding with 2400 grit SiC paper, mechanically polished with diamond suspensions of 6 μ m, 3 μ m and 1 μ m
25 followed by a chemical-mechanical polish with a mixture of 90 parts of colloidal silica (Struers OP-S) and 10
26 parts of hydrogen peroxide (30% Vol.).

27
28
29
30
31 For the prediction of the prevailing phases, their fractions and transition temperatures thermodynamic
32 equilibrium calculations based on CALPHAD (calculation of phase diagrams) were conducted with the
33 software MatCalc[®] using a commercially available database for TiAl [24].

38 3. Results and discussion

41 3.1. Characterization of TNM[™] powder

42
43
44 **Fig. 1** shows a SEM image of the microstructure of a TNM[™] powder particle taken in back-scattered
45 electron (BSE) mode. The microstructure exhibits a fine dendritic solidification structure which is a typical
46 feature of powders produced by gas atomization [14]. **Fig. 2a** shows the XRD pattern of the powder.
47 Obviously, it was not possible to “freeze-in” the β -phase, although gas atomization provides a high cooling
48 rate. So after dendritic solidification via the β -phase, i.e., $S \rightarrow S + \beta \rightarrow \beta$, the phase transformation $\beta \rightarrow \beta + \alpha$
49 can occur and the disordered high temperature phases β and α can partially order. The evaluation of the
50 XRD patterns using the Rietveld method leads to a volume fraction of 73% of α/α_2 -phase and 27% of β/β_0 -
51 phase. γ -phase was not observed. Due to the absence of superlattice peaks in the XRD pattern it is tempting
52 to speculate that due to the high cooling rates during gas atomization ($\sim 10^5$ K/s, see [14]) the ordering
53 reactions $\beta \rightarrow \beta_0$ and $\alpha \rightarrow \alpha_2$ could be suppressed. However, no further investigations were conducted
54
55
56
57
58
59
60
61
62
63
64
65

because the powder was not in the focus of this work and because the subsequent HIP process erases the history of the powder.

3.2. As-HIPed microstructure

During HIPing a fine-grained microstructure is formed consisting of almost equiaxed α_2 , β_0 and γ grains (**Fig. 3a**). These phases were identified in the as-HIPed condition by XRD measurements (**Fig. 2b**). The corresponding grain size distribution is shown in **Fig. 3b**. The average grain diameter of each phase was determined from three different SEM images employing the software AnalySIS[®]. To visualize the grain size distribution clearly, the grain diameters in **Fig. 3b** are divided into 0.5 μm intervals. In these intervals the cross sectional area of all grains is summed up for each phase separately and the corresponding area fraction was calculated. Such a representation of the data allows to comment on the grain size that covers the major part of the total cross sectional area for each phase and thus on the microstructural homogeneity. The HIPed microstructure shows a very high homogeneity with a narrow grain size distribution. The average grain size for γ -TiAl is 7 μm , for α_2 -Ti₃Al 4 μm and for β_0 -TiAl 2 μm . The phase fractions for the HIPed condition evaluated independently from SEM and LOM images as well as from XRD measurements (**Fig. 2b**) are similar as summarized in **Table 1**.

3.3. Nano-hardness and reduced elastic modulus of the constituting phases

Nanoindentation was performed in the As-HIPed microstructure on all individual phases, namely α_2 , β_0 and γ , using a Berkovich-shaped diamond indenter. The indentation was carried out in load-control mode with 5 loading-unloading segments and with a maximum indentation load of 5000 μN . The hardness and the reduced modulus were evaluated from the load-displacement curves by the Oliver-Pharr method similar to the procedures used in [25]. For each phase a total of 10-12 indents in 3-4 grains were performed to obtain acceptable statistical values of hardness and reduced modulus. The phases of the indented grains were identified after indentation by SEM investigation in BSE mode whereby α_2 , β_0 and γ were distinguished by their brightness in the SEM micrographs. An example is shown in **Fig. 3a**. In **Fig. 4a** the hardness values plotted against indentation depth are shown. It is evident from this graph that for the maximum load of 5000 μN , β_0 shows the smallest indentation depth with values between 40 and 120 nm followed by the α_2 and γ -phase that reach maximum indentation depths of 140 and 160 nm respectively. The evaluated hardness values are 4.2 GPa for γ -phase, 5.3 GPa for α_2 -phase and 7.2 GPa for the β_0 -phase. At these small indentation depths the phases showed no pronounced indentation size effect. Larger indentation depths were avoided as the hardness values could be affected by the neighbouring grains. The hardness value of 4.2 GPa for the γ -phase is in good accordance with other results published in literature [25,26]. The hardness of 5.3 GPa measured for the α_2 -phase is slightly lower than the values of 7.4 ± 0.5 GPa reported by [25] in a lamellar PST-TiAl alloy. One possible explanation for this difference is the fact that the measurements were carried out in different microstructures: Here we measured on a globular microstructure with a grain size of 5-6 μm , whereas in [25] the measurements were performed in α_2 -lamellae of approximately 1-2 μm width. In the latter, dislocation movement could be restricted by neighbouring interfaces, hence resulting in higher hardness values. The hardness value for the β_0 -phase is the highest of all phases, i.e. 7.2 GPa. To our knowledge no isolated measurements on hardness of the β_0 -phase are published in literature to this date.

1 Nevertheless, the high value of 7.2 GPa is reasonable for an ordered intermetallic phase. The reduced
2 modulus of 149 GPa determined for the α_2 -phase is in good accordance with the calculated value of 141
3 GPa along the $\langle 11\text{-}21 \rangle$ direction given by [27]. With 163 GPa the γ -phase has a slightly lower elastic
4 modulus than the experimental value of 185 GPa determined using Hill average from elastic constants of
5 single crystals for Ti-50 at% Al. by [27]. The calculated reduced modulus value for β_o -phase is around 172
6 GPa. Here as for the hardness of the β_o -phase no values are available in literature yet for comparison.
7
8
9

10 11 **3.4. Effect of annealing on phase fraction and grain size** 12 13

14 The fine-grained HIPed material as depicted in **Fig. 3a** represents the starting microstructure for subsequent
15 heat-treatments aiming at the adjustment of NL microstructures with a small colony size. The LOM images
16 compiled in **Fig. 5** show the evolution of the microstructure during annealing experiments in the temperature
17 range from 1230°C to 1350°C followed by AC, which leads to different effective cooling rates depending on
18 the used sample dimension. For heat-treatments up to 1285°C (**Fig. 5a-e**) the sample size of 5x5x5 mm³ is
19 small enough to “freeze-in” the high temperature microstructure during AC, thereby preserving the volume
20 fractions present at high temperature and preventing the formation of γ -lamellae from supersaturated α -
21 grains [28]. To detect the grain boundaries and microstructural constituents as shown in **Figs. 5b-e** the
22 samples have to be additionally thermal etched at 900°C for 2 minutes. During this procedure fine γ -lamellae
23 and γ -grains are precipitated in the supersaturated α_2 -grains and on their grain boundaries, visible in **Fig. 5b-**
24 **e**. This enables quantitative characterisation of microstructural constituents but preclude the detection of
25 phase fractions. The annealing experiments at 1290°C and 1350°C within the ($\alpha + \beta$)-phase field region
26 (**Figs. 5f-h**) were conducted on specimens with dimensions of 10x10x10 mm³. Due to the larger specimen
27 volume the cooling rate during AC to room temperature was lower than in the heat-treated samples shown in
28 **Figs. 5a-e**. As a result of the lower effective cooling rate the formation of γ -lamellae in the α -matrix could not
29 be suppressed (**Figs. 5f,g**). For example, the occurrence of fine γ -lamellae within α_2 -grains from AC is
30 illustrated in **Figs. 5f,g**. On the other hand, AC is slow enough to avoid cracking of the samples.
31
32
33
34
35
36
37
38
39
40
41
42

43 From **Fig. 5a** it is evident that the 1 hour annealing treatment at 1230°C was conducted in the ($\alpha + \beta_o + \gamma$)-
44 phase field region. With increasing temperature the volume fraction of the γ and β_o -phase decreases. After
45 annealing at 1250°C for 1 hour only α_2 -phase and γ -phase were detected but no β_o -phase (**Fig. 5b**). This
46 indicates that the heat-treatment was conducted in the ($\alpha+\gamma$)-phase field region. An increase of the annealing
47 temperature to 1260°C leads to a further decrease of the amount of γ -phase (**Fig. 5c**). Obviously, at 1260°C
48 $T_{\gamma\text{solv}}$ is already reached and a single α -phase field up to 1265°C (**Fig. 5d**) is present. It should be noted that
49 during annealing between 1230°C (**Fig. 5a**) and 1250°C (**Fig. 5b**) microstructures with a homogeneous
50 distribution of the constituting phases have been formed. Especially, the α -phase shows a uniform grain
51 growth behaviour during the 1 hour heat-treatments. Thus the temperature range of 10°C to 30°C below
52 $T_{\gamma\text{solv}}$ is from special interest, because it is suitable to produce NL+ γ microstructures with relatively small α_2 -
53 grains in the range of 10 to 45 μm , which, in a later heat-treatment step, can be transformed to lamellar α_2/γ -
54 colonies. In this temperature range (see section 3.5) the γ -phase fraction changes by about 1 vol.% per 1°C.
55
56
57
58
59
60
61
62
63
64
65

1 For example a change of the annealing temperature by 10°C from $T_{\gamma_{\text{solv}}}$ minus 20°C to $T_{\gamma_{\text{solv}}}$ minus 30°C
2 leads to a change in the globular γ -phase fraction from 20 to 30 vol.%. Above 1250°C (corresponding to $T_{\gamma_{\text{solv}}}$
3 minus 10°C) the γ -phase fraction shrinks to below 10 vol.% and the growth of particularly large α -grains
4 starts at sites where the γ -phase has already vanished (**Fig. 5c**).
5

6 In the single α -phase field region between 1260°C and 1265°C during a holding time of 1 hour excessive
7 grain growth takes place due to the absence of retarding phases (γ , β) (**Fig. 5d**). At 1285°C, in the (α + β)-
8 phase field, the excessive growth of the α -grains is hindered by the presence of about 3 vol.% β -phase in
9 combination with a short annealing time (**Fig. 5e**). From **Figs. 5e-g** it is evident that fine NL+ β
10 microstructures with a low nearly constant β -phase fraction can be formed through short-term annealing
11 treatments in the (α + β)-phase field region, approximately 30-60°C above $T_{\gamma_{\text{solv}}}$. Heat-treatments 90°C
12 above $T_{\gamma_{\text{solv}}}$ at 1350°C (**Fig. 5h**) lead to an increased fraction of β -phase which restricts the growth of α -
13 grains, even during extended holding times. A holding time of 30 minutes at 1350°C ($T_{\gamma_{\text{solv}}}+90^\circ\text{C}$) leads to a
14 uniform homogenous grain growth and an average α_2 -grain size of 35 μm . The sample, shown in **Fig. 5h**,
15 was oil quenched (OQ) to room temperature to inhibit the formation of γ -lamellae. The results clearly show
16 that in the chosen temperature range grain growth and microstructural homogeneity depend mainly on the
17 applied holding time and the present β -phase volume fraction. Annealing experiments with different holding
18 times at 1290°C have shown, that after 9 minutes/AC (**Fig. 5f**) as well as after 30 minutes/AC (**Fig. 5g**) the
19 microstructural fractions are more or less the same (α_2/γ -colonies: 96.5 vol.%; β_0 -phase: 3.5 vol.%). Thus,
20 grain size and the microstructural homogeneity were evaluated on these two samples (**Figs. 5f,g**). The
21 results are summarized in **Figs. 6a,b**.
22
23
24
25
26
27
28
29
30
31
32

33 In the LOM image (**Fig. 5g**) taken after 30 minutes at 1290°C a tendency of the grains to coarsen is visible.
34 The same trend is apparent from a comparison between the grain size distributions in **Fig. 6**. After 9 minutes
35 at 1290°C only one grain with a size of 87 μm was detected using the analysis of 10 LOM images (**Fig. 6a**),
36 whereas after 30 minutes at 1290°C several large grains of up to 135 μm in diameter were detected (**Fig.**
37 **6b**). The results show that NL+ β microstructures with a mean colony size of about 30 μm are achievable by
38 means of short term heat-treatments within the lower temperature limit of the (α + β)-phase field region.
39 However, the corresponding low β -phase fraction in the 3% range only prevents undesired grain growth
40 either for short annealing times or not at all. For longer holding times above $T_{\gamma_{\text{solv}}}$ a minimum β -phase
41 fraction of 10% is necessary to ensure controlled grain growth and a homogeneous grain size distribution
42 (**Fig. 5h**). Thus, it can be concluded that the microstructural quality depends strongly on the distribution of
43 the β -phase within the α -matrix and the optimum holding time at a fixed temperature depending on the
44 dimension of the sample and cooling rate.
45
46
47
48
49
50
51
52

53 **3.5. Calculated and experimental phase fraction diagram**

54 The good chemical homogeneity of the PM processed and heat-treated TNM™ alloy allows the comparison
55 of the experimentally obtained phase fraction diagram to the calculated one. The calculated phase fraction
56 diagram for the investigated alloy composition Ti-43.9Al-4.0Nb-0.95Mo-0.1B is shown in **Fig. 7a**. In recent
57
58
59
60
61
62
63
64
65

1 publications, however, the thermodynamic database used here was found to describe the transition
2 temperatures and phase proportions poorly in high Nb containing γ -TiAl based alloys as reported in [29,30].
3 Therefore, it should be pointed out that the calculation shown in **Fig. 7a** expresses trends for phase fractions
4 and transition temperatures rather than absolute values. The experimentally evaluated phase fractions from
5 LOM images, ex-situ XRD and in-situ HEXRD are summarized in **Fig. 7b**. From **Fig. 7b** it is evident that the
6 phase fractions obtained from LOM images of the heat-treated samples are in agreement with the in-situ
7 HEXRD results up to $T_{\gamma_{\text{solv}}}$. At temperatures above $T_{\gamma_{\text{solv}}}$, however, the HEXRD results show a higher β -
8 phase fraction than detected by LOM. Obviously, it was not possible to freeze-in the whole β -phase fraction
9 present at 1350°C. This result is consistent with the observation in the gas-atomized TNM™ powder (see
10 section 3.1). It is supposed that the high cooling rate provided by OQ triggers a martensitic $\beta \rightarrow \alpha$
11 transformation. An increase in holding time from 1 hour to 10 hours at temperatures higher than 1200°C
12 shows only a decrease of about 2 vol.% in the experimentally observed phase fraction of the β -phase,
13 determined by XRD as well as LOM. This observation, in combination with the HEXRD results at a heating
14 rate of 2 K/min, leads to the conclusion that dissolution and precipitation kinetics of the β -phase in this
15 temperature region is fast. Comparison between calculated and measured phase fractions and temperatures
16 shows the following:
17
18
19
20
21
22

- 23 - A small difference in the γ -solvus temperature can be recognized between the calculated and
24 experimentally derived data. The thermodynamic calculation predicts a $T_{\gamma_{\text{solv}}}$ slightly higher than it is
25 found experimentally.
- 26 - The course of the phase fractions around $T_{\gamma_{\text{solv}}}$ are in agreement with the calculated data.
- 27 - The calculated and measured phase fractions above and below $T_{\gamma_{\text{solv}}}$ differ increasingly with increasing
28 distance to $T_{\gamma_{\text{solv}}}$. Interestingly, the experimentally determined phase fractions are in agreement with
29 the calculated data after an additional precipitation annealing treatment at 850°C/6 h/FC (see section
30 3.6).
- 31 - The existence of the predicted small single α -phase field at 1275°C was experimentally confirmed by
32 the results of the 1 hour heat-treatments between 1260°C and 1265°C (**Fig. 5d**) as well as in in-situ
33 HEXRD investigations.
- 34 - The determined temperature dependence of the β -phase fraction fits satisfactorily between experiment
35 and calculation in the vicinity of $T_{\gamma_{\text{solv}}}$.

36
37
38
39
40
41
42
43
44
45
46
47 Altogether, these results show that thermodynamic calculations reflect the qualitative trends of the
48 temperature dependence of phase fractions around $T_{\gamma_{\text{solv}}}$ rather well. Nevertheless, for more exact
49 quantitative calculations the thermodynamic database for TiAl with high Nb (and Mo) contents must be
50 further improved, as recently reported for Nb-rich γ -TiAl alloys [30,31].
51
52
53

54 **3.6. Influence of cooling rate and ageing treatments on the formation of nearly lamellar** 55 **microstructures and macro-hardness** 56

57
58
59 In order to understand the formation of NL+ β microstructures annealing treatments were conducted at
60 1290°C for 9 min and 12 min followed by cooling to room temperature with different rates (AC and WQ). The
61
62
63
64
65

1
2
3
4
5
6
7
8
9
10
11
12
13
14
15
16
17
18
19
20
21
22
23
24
25
26
27
28
29
30
31
32
33
34
35
36
37
38
39
40
41
42
43
44
45
46
47
48
49
50
51
52
53
54
55
56
57
58
59
60
61
62
63
64
65

three heat-treatments, designated HT 1-3, are listed in **Table 1**. HT1 and HT2 were conducted on HIPed samples with dimensions 10×10×10 mm³, whereas HT3 was performed on larger specimens (Ø44 mm x 20 mm). Therefore, it must be noted that the different sample types experience different cooling rates, as far as AC is concerned. However, the larger specimens are needed to provide material for characterizing the mechanical properties.

Since WQ after HT1 (1290°C/9 min/WQ) provides a high cooling rate, the precipitation of γ -laths both in the α and β -phase can be suppressed as shown in **Fig. 8a**. In **Fig. 2c** the XRD pattern derived from the HT1 sample is depicted. The peaks of α_2 and β_o -phase are clearly visible and the volume fractions determined by Rietveld analysis amount to 95 vol.% α_2 and 5 vol.% β_o -phase. No γ -phase was observed. In contrast the XRD patterns taken after HT2 (1290°C/9 min/AC) with a significantly lower cooling rate shows clear peaks that are related to the γ -phase (**Fig. 2d**). According to the Rietveld analysis the volume fraction of γ , α_2 and β_o -phase is 44%, 53% and 3%, respectively (**Table 1**). Obviously, during WQ (HT1) about 2 vol.% more former β -phase could be preserved than during AC (HT2), see **Table 1**. However, WQ from 1290°C induces micro-cracks so that this route cannot be used to provide defect-free specimens for, e.g., mechanical testing. At the lower cooling rate of AC during HT2, however, micro-cracks can be avoided. During HT2 fine γ -lamellae precipitate in the former α -grains forming α_2/γ -colonies. Additionally, a small amount of β_o -phase transforms to γ , which either decorates the grain boundaries of the β_o -grains (see inset in **Fig. 8b**) or forms small γ -platelets inside the β_o -grains exhibiting specific crystallographic relationships [12,32,33]. As already mentioned HT3 (1290°C/12 min/AC + 850°C/6 h/FC) was carried out on a larger sample. The second heat-treatment step in HT3, i.e. annealing at 850°C for 6 h followed by FC, leads to the precipitation of more γ -lamellae in the oversaturated α_2 -grains. Additionally, the start of the cellular (discontinuous) reaction can be observed at the boundaries of α_2/γ -colonies as well as in form of the precipitation of more lens-shaped γ -platelets in the β_o -phase (see **Fig. 8c** and inset). An identical behaviour was observed for a TNM™ alloy which was cast, hot-forged and heat-treated [8]. The increase in the content of γ -phase is also evident in the XRD pattern (**Fig. 2e**). According to Rietveld analysis the difference between the γ -phase fraction of HT2 and HT3 is 25 vol.% (**Table 1**).

The TEM image in **Fig. 9** shows an example of the fine lamellar spacing within the α_2/γ -colonies after HT3. For HT 3 the mean interface spacing, averaged over 979 α_2/γ - and γ/γ -interfaces in 5 grains, was determined to be approximately 24 ± 18 nm. The large standard deviation suggests large variations in the measured distances. Large variations were found among different grains and even within the same grain. The image in **Fig. 9** provides an example of two regions within the same grain that exhibit clear and large differences in lamellar spacings. Nevertheless, we assume that the 6 hour ageing treatment at 850°C has established a state in the material closer to thermodynamic equilibrium. The calculated phase fractions are in good accordance with the experimental ones at these temperature and heat treatment conditions (**Fig. 7**). The ageing treatment at 850°C has also triggered the onset of the cellular reaction at α_2/γ -colony boundaries (**Fig. 8c**). From the inset of **Fig. 8c** it is evident that the cellular reaction leads to a partial breakdown of the lamellar colonies. The driving force of the cellular reaction stems from the strong chemical imbalance due to relatively fast cooling from 1290°C as well as from the high interface energy resulting from the presence of a very fine lamellar structure during the annealing step at 850°C for 6 hours [15,34]. Finally, **Table 1**

1 summarizes the results from XRD and quantitative SEM/LOM analysis. It should be kept in mind that SEM
2 and LOM images have a certain resolution limit. Consequently, very small features of the microstructure,
3 e.g., fine γ -TiAl laths in α_2/γ -colonies, which are below the resolution limit of SEM and LOM are not included
4 in the evaluation. This information can be gained from XRD measurements which yield the total amounts of
5 phase fractions. In this case, however, no assignment to specific constituents of the microstructure can be
6 made, e.g. no distinction between γ -grains or γ -lamellae. However, from **Table 1** it is evident, that both
7 methods provide complementary results [35]. For example, the volume fraction of the α_2/γ -colonies and the
8 β_0 -grains does not change during HT2 and HT3 (**Figs. 8b,c**), meaning that no change at macroscopic level
9 has taken place. Nevertheless, XRD measurements (**Table 1**) clearly show a significant change in phase
10 fraction, accompanied by microstructural change on the sub- μm scale, which can be related to further
11 precipitations of γ -phase in α_2 -grains (α_2/γ -colonies) as well as in β_0 -grains.
12
13
14
15
16

17 In addition, **Table 1** summarizes the results of macro-hardness measurements conducted on samples
18 showing different microstructures (HIP, HT1-3). The as-HIPed condition, exhibiting a fine-grained equiaxed
19 microstructure (**Fig. 3a**), shows the lowest hardness (333 HV10). After heat-treatment HT1
20 (1290°C/9 min/WQ), which leads at room temperature to a γ -free ($\alpha_2 + \beta_0$) microstructure (**Fig. 8a**), the
21 material exhibits the highest hardness (454 HV10). If the same heat-treatment is performed with subsequent
22 AC (HT2) the hardness reaches a lower value of 435 HV10. HT3 includes an additional ageing treatment at
23 850°C for 6 hours followed by FC which is accompanied by a further slight decrease of the macro-hardness
24 (412 HV10) compared to HT1 and HT2.
25
26
27
28
29
30

31 To explain the differences in hardness determined for NL+ β microstructures after heat-treatments HT1, HT2
32 and HT3 it is necessary to take into account the different microstructures and sample sizes. After WQ
33 performed as last step of HT1 a γ -free microstructure is obtained with high residual stresses which lead to
34 crack initiation. This, and a possible solute solution hardening effect in the supersaturated α_2 -phase, most
35 probably explains the high hardness after HT1. After AC as last step of HT2 fine γ -lamellae are present in the
36 α_2/γ -colonies. Due to the increase of γ -phase to 44 vol.% accompanied by the relaxation of residual stresses
37 during AC, the hardness decreases compared to HT1. The hardening by the introduction of additional γ/α_2 -
38 interfaces in the colonies does not compensate this.
39
40
41
42
43

44 The slight decrease of macro-hardness in HT3 compared to HT2 results from different sample size. Due to
45 the larger sample size in HT3 a slower cooling rate during AC in the first heat-treatment step was reached.
46 Thereby, broader γ -lamellae precipitated in the larger sample of HT3 [28]. After the second heat-treatment
47 step at 850°C for 6 hours (HT3), the volume fraction of γ -lamellae increases to 69% but it was not possible to
48 reach such a fine lamellae structure than in HT2. This leads to the further observed decrease of hardness
49 after HT3. The phase fractions calculated by means of Rietveld analysis of the HIPed sample and after HT3
50 are not very different (see **Table 1**). Although the content of the harder β_0 -phase is higher in the HIPed
51 condition than after HT3, the macro-hardness is considerably lower. This results merely from the
52 arrangement of the γ -phase within the microstructure. In the HIPed material the γ -phase forms equiaxed
53 grains, whereas in the HT3 condition the γ -phase is present within the lamellar colonies. For further
54 information concerning the relationship between macro-hardness and microstructure in TNM™ alloys the
55
56
57
58
59
60
61
62
63
64
65

reader is referred to a recent paper by Cha et al. [10]. Details about the mechanical properties of lamellar microstructures are found in literature [11,36,37,38].

4. Summary

A powder metallurgical processed TNM™ alloy with a composition of Ti-43.9Al-4.0Nb-0.95Mo-0.1B was used to adjust nearly lamellar microstructures by means of two-step heat-treatments. The evaluation of the microstructure was determined by LOM, SEM, TEM, XRD, HEXRD as well as macro- and nano-hardness measurements. During the HIP process of the TNM™ powder a fine-grained globular microstructure with a narrow grain size distribution is formed. The dominant γ -phase exhibits an average grain size of 7 μm and the macro-hardness of the HIPed condition is 333 HV10. The individual hardness values and reduced modulus of the constituting phases were determined by means of nanoindentation. The nano-hardness measurements result in 4.2 GPa for γ , 5.2 GPa for α_2 and 7.5 GPa for β_o , respectively. The reduced modulus was determined to be 163 GPa for γ , 149 GPa for α_2 and 172 GPa for β_o .

The HIPed microstructure offers the possibility to adjust fine-grained nearly lamellar microstructures. The studies have shown how different NL+ γ microstructures which a colony size in the range of 10 to 45 μm can be adjusted by annealing below $T_{\gamma\text{solv}}$. For NL+ β microstructures, the β -phase fraction and the holding time are the crucial factors in preventing grain growth. NL+ β microstructures with a low β_o -amount (3 vol.%) and a mean colony size of about 30 μm are obtained by means of a short-term heat-treatment (9 min at 1290°C), which corresponds to a temperature of 30°C above $T_{\gamma\text{solv}}$. An increase of holding time up to 30 min at $T_{\gamma\text{solv}}+30^\circ\text{C}$ leads to fast grain growth with a grain size up to 135 μm as a consequence of the low β -phase content on the α -grain boundaries. In contrast, fine NL+ β microstructures with an average α_2/γ -colony size of 35 μm and uniform homogenous grain growth can be adjusted with a holding time of 30 minutes at $T_{\gamma\text{solv}}+90^\circ\text{C}$. Here, a minimum β -phase fraction of 10 vol.% is necessary to ensure controlled grain growth.

To evaluate the microstructural development as a function of temperature, phase fractions and microstructural constituents of different heat-treated samples were evaluated by means of quantitative metallography and conventional XRD. These results match well with the data derived from in-situ HEXRD measurements. Additionally, the experimentally observed dependency of the phase fractions on temperature was compared with those derived from thermodynamic calculations employing a commercially available TiAl data base. However, a satisfying agreement between the results was only found in the vicinity of $T_{\gamma\text{solv}}$.

The microstructure development of NL+ β microstructures during two-step heat-treatments was evaluated in detail. The phase fractions and macro-hardness occurring after the first heat-treatment step were determined for different cooling rates from 1290°C. Water quenching leads to a γ -free microstructure at room temperature which consists of α_2 and β_o -grains. Through the presence of residual stresses, which also leads to the formation of micro-cracks, the macro-hardness is increased to 454 HV10 when compared to the HIPed microstructure. Air cooling from 1290°C leads to a lower average macro-hardness of 435 HV10 because of lower residual stresses. The precipitation of 44 vol.% γ -phase in form of fine lamellae, however, could not compensate the hardness loss due to stress release. After a final ageing treatment at 850°C for 6 hours the

adjustment of the nearly lamellar microstructure is finished. The NL+ β microstructure has a hardness of 412 HV10 and the average interface spacing in the α_2/γ -colonies is 24 ± 18 nm. During ageing the γ -phase within the lamellar colonies increased to 69 vol.%.

Acknowledgements

A part of this study was conducted within the framework of the BMBF project O3X3530A, Germany, and the Styrian Materials Cluster, Austria. The support of the DESY management, User Office and beamline staff is highly acknowledged. Research activities leading to the presented results received funding from the European Community's Seventh Framework Programme (FP7/2007-2013) under grant agreement no. 226716.

References

- [1] Y.-W. Kim, Development of beta gamma alloys: Opening robust processing and greater application potential for TiAl-based alloys, in: Y.-W. Kim, D. Morris, R. Yang, C. Leyens (Eds.), Structural Aluminides for Elevated Temperatures, The Minerals, Metals & Materials Society, Warrendale, 2008, pp. 215.
- [2] T. Tetsui, The effect of composition on the endurance of TiAl alloys in turbocharger applications, in: Y.-W. Kim, D. M. Dimiduk, M. H. Loretto (Eds.), Gamma Titanium Aluminides 1999, The Minerals, Metals & Materials Society, Warrendale, 1999, pp.15–23.
- [3] B. P. Bewlay, Presentation at the European symposium on superalloys and their applications, Wildbad Kreuth, Germany, May 25-28 (2010).
- [4] H. Clemens, H. Chladil, W. Wallgram, G. Zickler, R. Gerling, K.-D. Liss, S. Kremmer, V. Güther, W. Smarsly, In and ex situ investigations of the β -phase in a Nb and Mo containing γ -TiAl based alloy, *Intermetallics*, vol. 16 (2008) 827–833.
- [5] H. Clemens, W. Wallgram, S. Kremmer, V. Güther, A. Otto, A. Bartels, Design of novel β -solidifying TiAl alloys with adjustable β /B2-phase fraction and excellent hot-workability, *Advanced Engineering Materials*, vol. 10 (2008) 707–713.
- [6] H. Chladil, H. Clemens, A. Ottand, V. Güther, S. Kremmer, A. Bartels, R. Gerling, Charakterisierung einer β -erstarrenden γ -TiAl-Basislegierung, *BHM*, vol. 9 (2006) 356–361.
- [7] V. Küstner, M. Oehring, A. Chatterjee, V. Güther, H.-G. Brokmeier, H. Clemens, F. Appel, An investigation of microstructure formation during solidification of gamma Titanium Aluminide alloys, in: Y. W. Kim, H. Clemens, A. H. Rosenberger (Eds.), Gamma Titanium Aluminides 2003, The Minerals, Metals & Materials Society, Warrendale, 2003, pp. 89–96.
- [8] W. Wallgram, T. Schmörlzer, L. Cha, G. Das, V. Güther, H. Clemens, Technology and mechanical properties of advanced γ -TiAl based alloys, *International Journal of Materials Research*, vol. 100 (2009) 1021–1030.
- [9] F. Appel, J. D. H. Paul, M. Oehring, H. Clemens, F. D. Fischer, Physical metallurgy of high Nb-containing TiAl alloys, *International Journal of Materials Research*, vol. 95 (2004) 585–591.
- [10] L. Cha, H. Clemens, G. Dehm, Microstructure evolution and mechanical properties of an intermetallic Ti-43.5Al-4Nb-1Mo-0.1B alloy after aging below the eutectoid temperature, *International Journal of Materials*, vol. 102 (2011) 703–708.
- [11] G. Dehm, C. Motz, C. Scheu, H. Clemens, P. H. Mayerhofer, C. Mitterer, Mechanical size-effects in miniaturized and bulk materials, *Advanced Engineering Materials*, vol. 8 (2006) 1033–1045.
- [12] L. M. Droessler, T. Schmoelzer, W. Wallgram, L. Cha, G. Das, H. Clemens, Microstructure and tensile ductility of a Ti-43Al-4Nb-1Mo-0.1B alloy, *Materials Research Society Symposium Proceedings*, vol. 1128, 2009.
- [13] A. Bartels, C. Koeppe, H. Mecking, Microstructure and properties of Ti-48Al-2Cr after thermomechanical treatment, *Materials Science and Engineering*, vol. A192/193 (1995) 226–232.
- [14] R. Gerling, H. Clemens, F.-P. Schimansky, Powder metallurgical processing of intermetallic gamma Titanium Aluminides, *Advanced Engineering Materials*, vol. 6 (1996) 23–38.
- [15] M. Schloffer, Characterisation of microstructure development in Hot-die forged TNMTM-Titanaluminid, Diplomathesis, Montanuniversität Leoben, 2010.
- [16] J. Seeger, J. Klein, H. Mecking, Colour metallography of the intermetallic phases γ -TiAl und α_2 -Ti₃Al, *Praktische Metallographie*, vol. 27 (1990) 236–241.

- 1
2
3
4
5
6
7
8
9
10
11
12
13
14
15
16
17
18
19
20
21
22
23
24
25
26
27
28
29
30
31
32
33
34
35
36
37
38
39
40
41
42
43
44
45
46
47
48
49
50
51
52
53
54
55
56
57
58
59
60
61
62
63
64
65
- [17] K.-D. Liss, A. Bartels, A. Schreyer, H. Clemens, High-energy x-rays: A tool for advanced bulk investigations in materials science and physics, *Textures and Microstructures*, vol. 35 (2003) 219–252.
- [18] T. Lippmann, L. Lottemoser, F. Beckmann, R. Martins, T. Dose, R. Kirchhof, A. Schreyer, Hasylab annual report, Hasylab/DESY, Hamburg, Tech. Rep. 113, 2007.
- [19] W. Reimers, A. R. Pyzalla, A. Schreyer, H. Clemens, *Neutrons and Synchrotron Radiation in Engineering Materials Science*, Wiley-VCH, Weinheim, Germany, 2008.
- [20] A. Stark, M. Oehring, F. Pyczak, A. Schreyer, In situ observation of various phase transformation paths in Nb-rich TiAl alloys during quenching with different rates, *Advanced Engineering Materials* vol. 13 (2011) 700-704.
- [21] A.P. Hammersley, S.O. Svensson, M. Hanfland, A.N. Fitch, D. Häsermann, Two-dimensional detector software: From real detector to idealised image or two-theta scan, *High Pressure Research*, vol. 14 (1996) 235–248.
- [22] K.-D. Liss, A. Bartels, H. Clemens, S. Bystrzanowski, A. Stark, T. Buslaps, F.-P. Schimansky, R. Gerling, C. Scheu, A. Schreyer, Recrystallization and phase transitions in a γ -TiAl-based alloy as observed by ex situ and in situ high-energy x-ray diffraction, *Acta Materialia*, vol. 54 (2006) 3721 – 3735.
- [23] T. Novoselova, S. Malinov, W. Sha, A. Zhecheva, High-temperature synchrotron x-ray diffraction study of phases in a gamma TiAl alloy, *Materials Science and Engineering*, vol. A 371 (2004) 103–112.
- [24] N. Saunders, Phase equilibria in multi-component γ -TiAl based alloys, in: Y.-W. Kim, D. M. Dimiduk, M. H. Loretto (Eds.), *Gamma Titanium Aluminides 1999*, The Minerals, Metals & Materials Society, Warrendale, 1999, pp. 183–188.
- [25] M. Göken, M. Kempf, W. D. Nix, Hardness and modulus of the lamellar microstructure in PST-TiAl studied by nanoindentations and AFM, *Acta Materialia*, vol. 49 (2001) 903 – 911.
- [26] S. Gebhard, F. Pyczak, M. Göken, Microstructural and micromechanical characterisation of TiAl alloys using atomic force microscopy and nanoindentation, *Materials Science and Engineering*, vol. 523 (2009) 235–241.
- [27] K. Tanaka, M. Koiwa, Single-crystal elastic constants of intermetallic compounds, *Intermetallics*, vol. 4 (1996) 29 – 39.
- [28] M. Schloffer, H. Clemens, S. Mayer, Precipitation of γ -lamellae in supersaturated α -Ti₃Al, Unpublished data, 2011.
- [29] H. Chladil, H. Clemens, H. Leitner, A. Bartels, R. Gerling, F.-P. Schimansky, S. Kremmer, Phase transformations in high niobium and carbon containing γ -TiAl based alloys, *Intermetallics*, vol. 14 (2006) 1194–1198.
- [30] H. Chladil, H. Clemens, G. A. Zickler, M. Takeyama, E. Kozeschnik, A. Bartels, T. Buslaps, R. Gerling, S. Kremmer, L. Yeoh, K.-D. Liss, Experimental studies and thermodynamic simulation of phase transformations in high Nb containing γ -TiAl based alloys, *International Journal of Materials Research*, vol. 98 (2007) 1131–1137.
- [31] Y. Liu, E. Gamsjäger, H. Clemens, Thermodynamic description of niobium-rich γ -TiAl alloys, *International Journal of Materials Research*, vol. 102 (2011) 692–696.
- [32] Z. Huang, Ordered omega phases in a 4Zr–4Nb-containing TiAl-based alloy, *Acta Materialia*, vol. 56 (2008) 1689–1700.
- [33] Z. Huang, D. Zhu, Thermal stability of Ti-44Al-8Nb-1B alloy, *Intermetallics*, vol. 16 (2008) 156–167.
- [34] A. Denquin, S. Naka, Phase transformation mechanisms involved in two-phase TiAl-based alloys-II. discontinuous coarsening and massive-type transformation, *Acta Materialia*, vol. 44 (1996) 353–365.
- [35] M. Schloffer, T. Schmölzer, S. Mayer, E. Schwaighofer, G. Hawranek, F.-P. Schimansky, F. Pyczak, H. Clemens, Charakterisierung einer pulvermetallurgisch hergestellten TNM-Titanaluminid-Legierung mittels komplementärer quantitativer Methoden, in: A. Kneissl, H. Clemens (Eds.), *Fortschritte in der Metallographie*, vol. 42. MAT INFO Werkstoff- Informationsgesellschaft, Sonderbände der Praktischen Metallographie, April 2010, pp. 239–244.
- [36] F. Appel, R. Wagner, Microstructure and deformation of two-phase γ -titanium aluminides, *Materials Science and Engineering*, vol. 22 (1998) 187–268.
- [37] F. Appel, M. Oehring, R. Wagner, Novel design concepts for γ -base titanium aluminide alloys, *Intermetallics*, vol. 8 (2000) 1283–1312.
- [38] G. Cao, L. Fu, J. Lin, Y. Zhang, C. Chen, The relationships of microstructure and properties of a fully lamellar TiAl alloy, *Intermetallics*, vol. 8 (2000) 647–653.

Table:

Table 1: Fraction of microstructural constituents and phases for different heat-treatments and cooling rates. The volume fractions of the microstructural constituents were determined from SEM/LOM images, where the phase fractions were obtained from XRD measurements. In addition, the results of macro-hardness measurements according to Vickers HV10 are given. The average of 5-10 HV10 imprints with the particular deviation is listed.

Figures:

Fig. 1: Microstructure of a Ti-43.9Al-4.0Nb-0.95Mo-0.1B powder particle produced by gas atomization. SEM image taken in BSE mode. The darker substructure shows the dendritic structure formed during solidification. The observed contrast results from differences in the chemical composition during dendritic solidification (see text).

Fig. 2: XRD patterns of Ti-43.9Al-4.0Nb-0.95Mo-0.1B a) as gas atomized powder (0–180 μm), b) in the as HIPed condition and c-e) after subsequent heat-treatments. The parameters and phase fractions (vol. %) are summarized at each graph, details are listed in **Table 1**; c) WQ in HT1 from 1290°C has suppressed the formation of γ -phase; d) AC in HT2 could not suppress the formation of γ -phase; e) During an additional ageing treatment after AC at 850°C for 6 hours (HT3) the γ -phase fraction increased.

Fig. 3: a) Microstructure of the HIPed Ti-43.9Al-4.0Nb-0.95Mo-0.1B powder consisting of globular γ -grains (dark contrast), α_2 -grains (grey contrast) and β_o -grains (bright contrast). SEM image taken in BSE mode. b) Grain size distribution of the HIPed microstructure.

Fig. 4: Local mechanical properties of the constituent phases in TNM™ alloy probed by nanoindentation. a) Hardness as a function of contact depth for α_2 , β_o and γ phase. b) Reduced modulus of elasticity for α_2 , β_o and γ phase. c) AFM picture which shows the topography of phases and nanoindents. The darkest phase is γ -phase, light dark is α -phase and bright phase is β_o -phase.

Fig. 5: Microstructure of HIPed Ti-43.9Al-4.0Nb-0.95Mo-0.1B alloy after different heat-treatments: a) 1230°C/1 h/AC; b) 1250°C/1 h/AC; c) 1260°C/1 h/AC; d) 1265°C/1 h/AC; e) 1285°C/9 min/AC; f) 1290°C/9 min/AC; g) 1290°C/30 min/AC; h) 1350°C/30 min/OQ. LOM images a-d) were taken on colour-etched samples. Images e-h) were taken in interference contrast using circular polarized light. The heat-treatment c) and d) was conducted in the single α -phase field region. In this case the appearing small second phases are borides. Due to additional thermal etching grain boundaries and lamellae are slightly visible in b) - e). For f) and g) the annealing treatment was conducted in the ($\alpha + \beta$) phase field region. The precipitation of γ -laths within the α -grains took place during AC, thus forming lamellar α_2/γ -colonies. The β_o -phase is mainly arranged along the α_2 -grain boundaries, but β_o -particles can be found in the interior of α_2 -grains too (see arrows in g)). In h) the fine grained microstructure consists of oversaturated α_2 -grains and a high fraction of β -phase along the α_2 -grain boundaries.

Fig. 6: Size distribution of the α_2/γ -colonies after annealing at 1290°C for a) 9 min and b) 30 min, following AC. The corresponding LOM images are shown in Figs. 5 f,g.

Fig. 7: a) Calculated phase fractions as a function of temperature for Ti-43.9Al-4.0Nb-0.95Mo-0.1B. b) The results of quantitative analysis of heat-treated samples (solid symbols) and in situ HEXRD measurements (open symbols).

1
2
3
4
5
6
7
8
9
10
11
12
13
14
15
16
17
18
19
20
21
22
23
24
25
26
27
28
29
30
31
32
33
34
35
36
37
38
39
40
41
42
43
44
45
46
47
48
49
50
51
52
53
54
55
56
57
58
59
60
61
62
63
64
65

Fig. 8: Microstructure of alloy Ti-43.9Al-4.0Nb-0.95Mo-0.1B after different heat-treatments: a) HT1 (1290°C/9 min/WQ), b) HT2 (1290°C/9 min/AC) and c) HT3 (1290°C/12 min/AC + 850°C/6 h/FC). SEM images taken in BSE mode. The appearing microstructural constituents are indicated. The insets show microstructural features in higher magnification (see text). Additionally, the average macro-hardness according to HV10 is indicated.

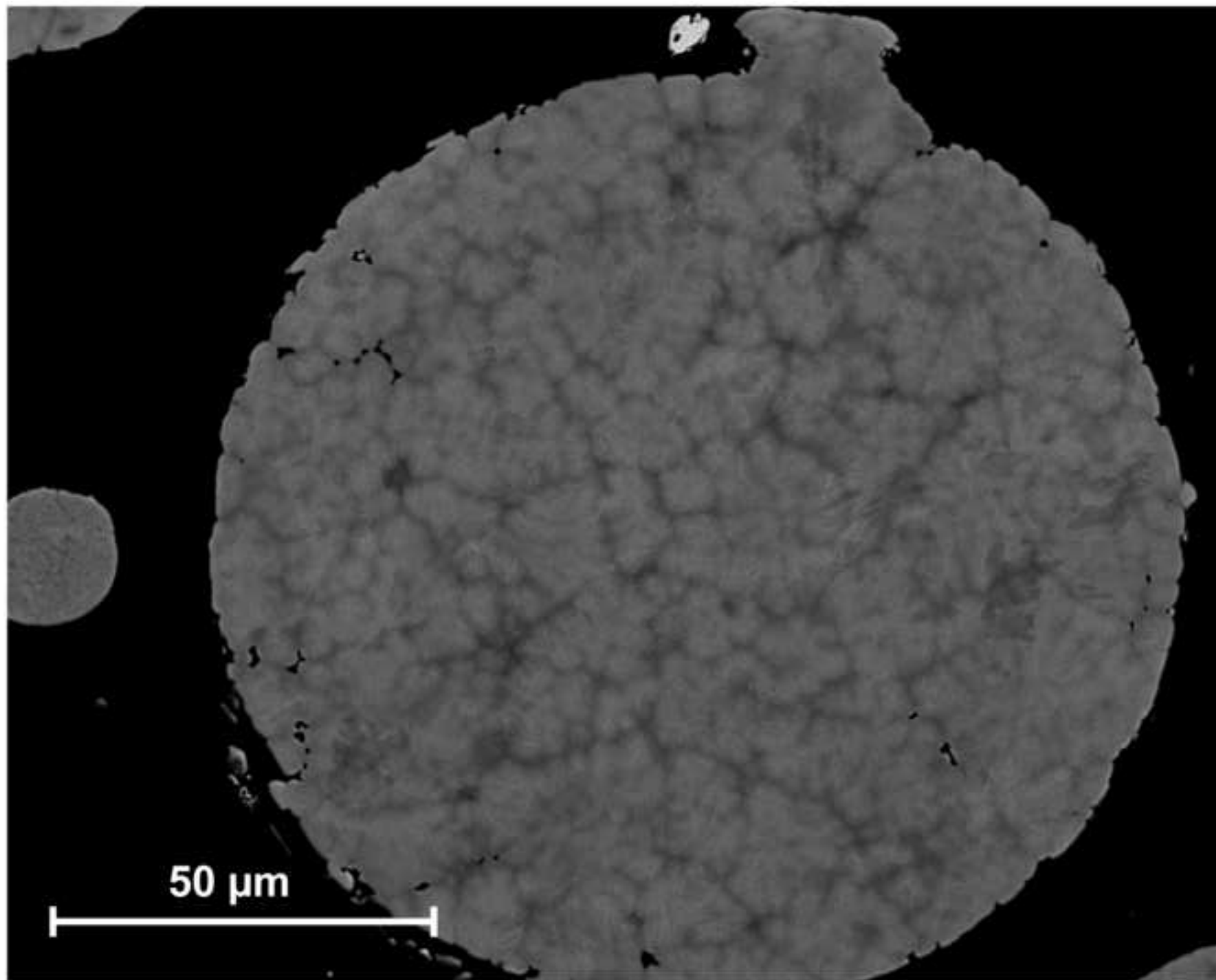
Fig. 9: TEM image of a lamellar α_2/γ -colony after HT3. The image shows two regions of the same grain projected along a $\langle 110 \rangle$ zone axis of the γ -phase, lamellas are seen edge-on. Large variations in lamellae spacings are apparent, the average interface spacing for HT 3 is 24 ± 18 nm.

Table(s)

[Click here to download high resolution image](#)

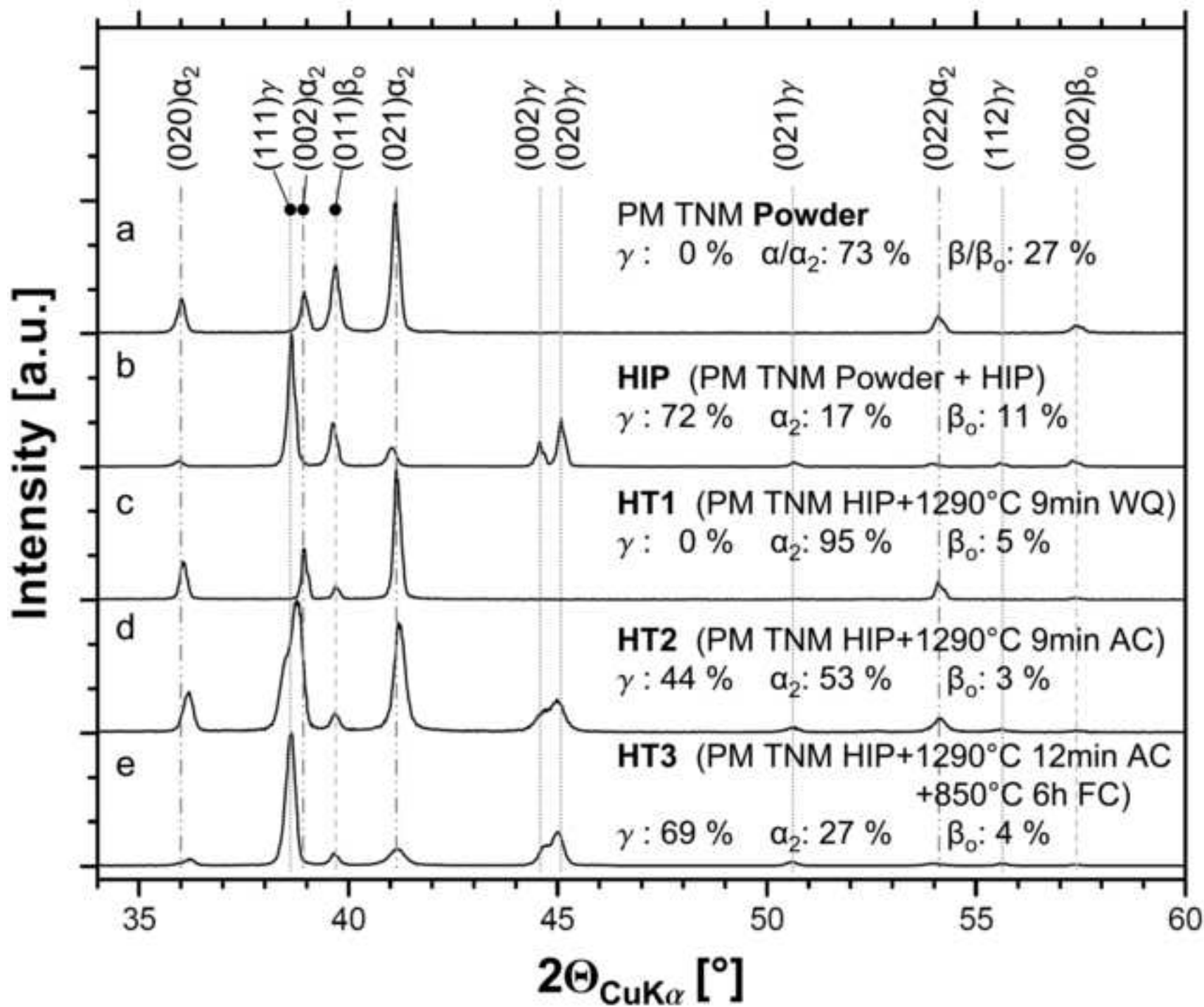
heat-treatment		microstructure	fraction of microstructural constituents SEM/LOM [vol. %]			phase fraction XRD [vol. %]			hardness HV10
HIP	HIP = 1250°C 2 h 200 MPa	globular triplex	γ -globular	α_2 -globular	β_0 -phase	γ -phase	α_2 -phase	β_0 -phase	333 \pm 5
			67 \pm3	19 \pm2	14 \pm1	72 \pm3	17 \pm3	11 \pm3	
HT1	HIP + 1290°C 9 min WQ	$\alpha_2 + \beta_0$	γ -globular	α_2 -grain	β_0 -phase	γ -phase	α_2 -phase	β_0 -phase	454 \pm 3
			0	95 \pm1	5 \pm1	0	95 \pm3	5 \pm3	
HT2	HIP + 1290°C 9 min AC	NL+ β	γ -globular	α_2/γ -colony	β_0 -phase	γ -phase	α_2 -phase	β_0 -phase	435 \pm 10
			0	97 \pm1	3 \pm1	44 \pm3	53 \pm3	3 \pm3	
HT3	HIP + 1290°C 12 min AC + 850°C/6h/FC	NL+ β	γ -globular	α_2/γ -colony	β_0 -phase	γ -phase	α_2 -phase	β_0 -phase	412 \pm 5
			0	96 \pm1	4 \pm1	69 \pm3	27 \pm3	4 \pm3	

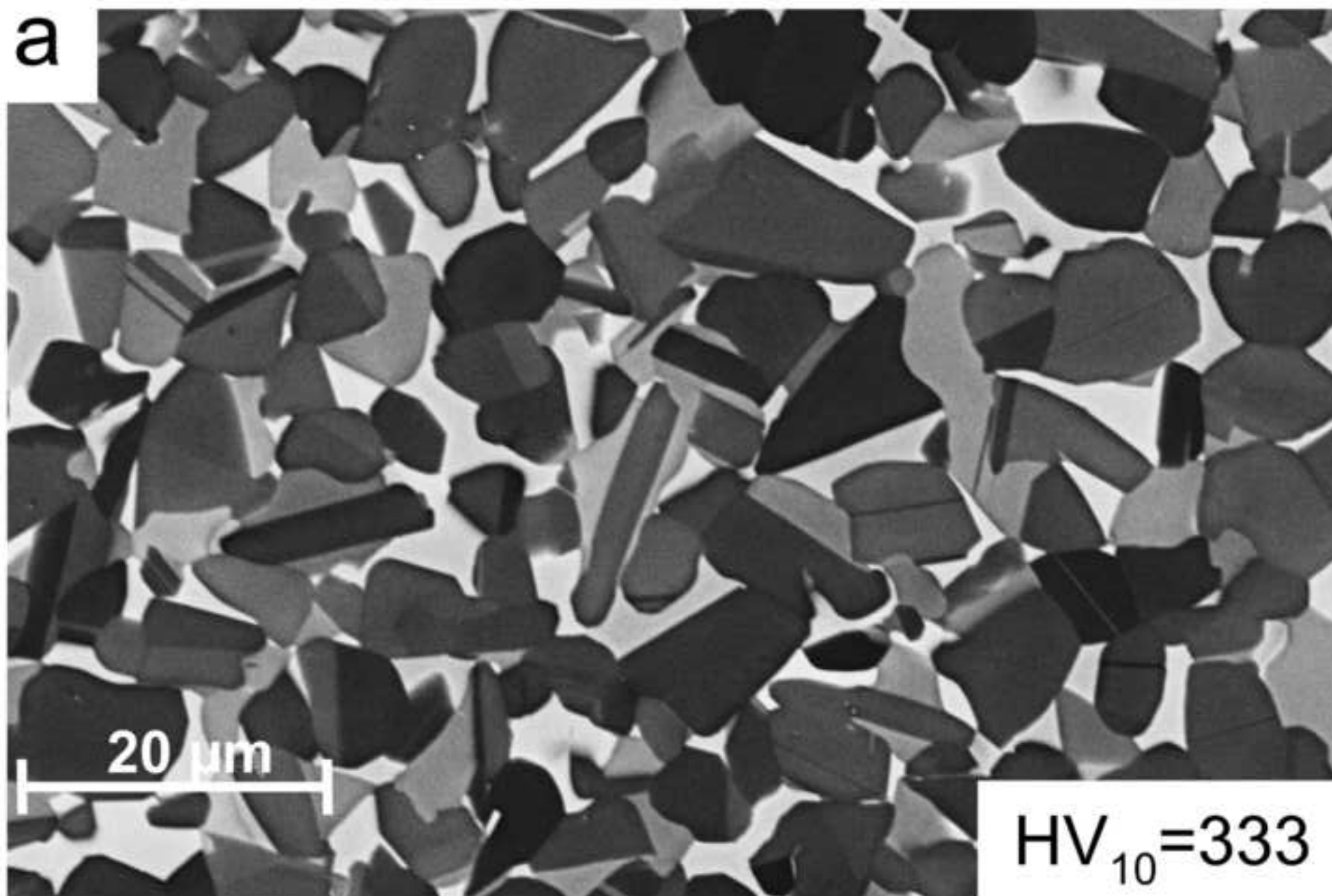
Figure(s)
[Click here to download high resolution image](#)



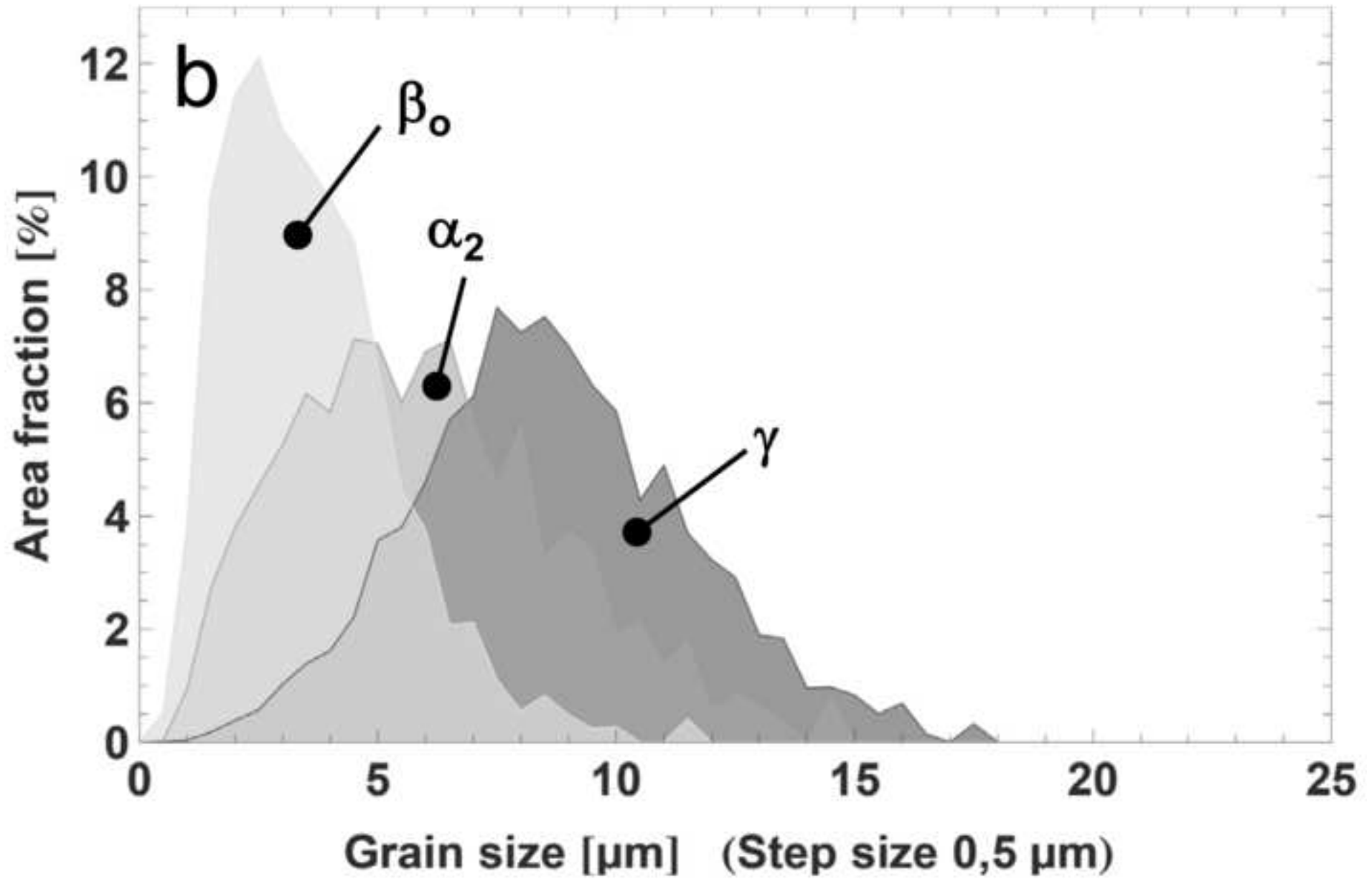
Figure(s)

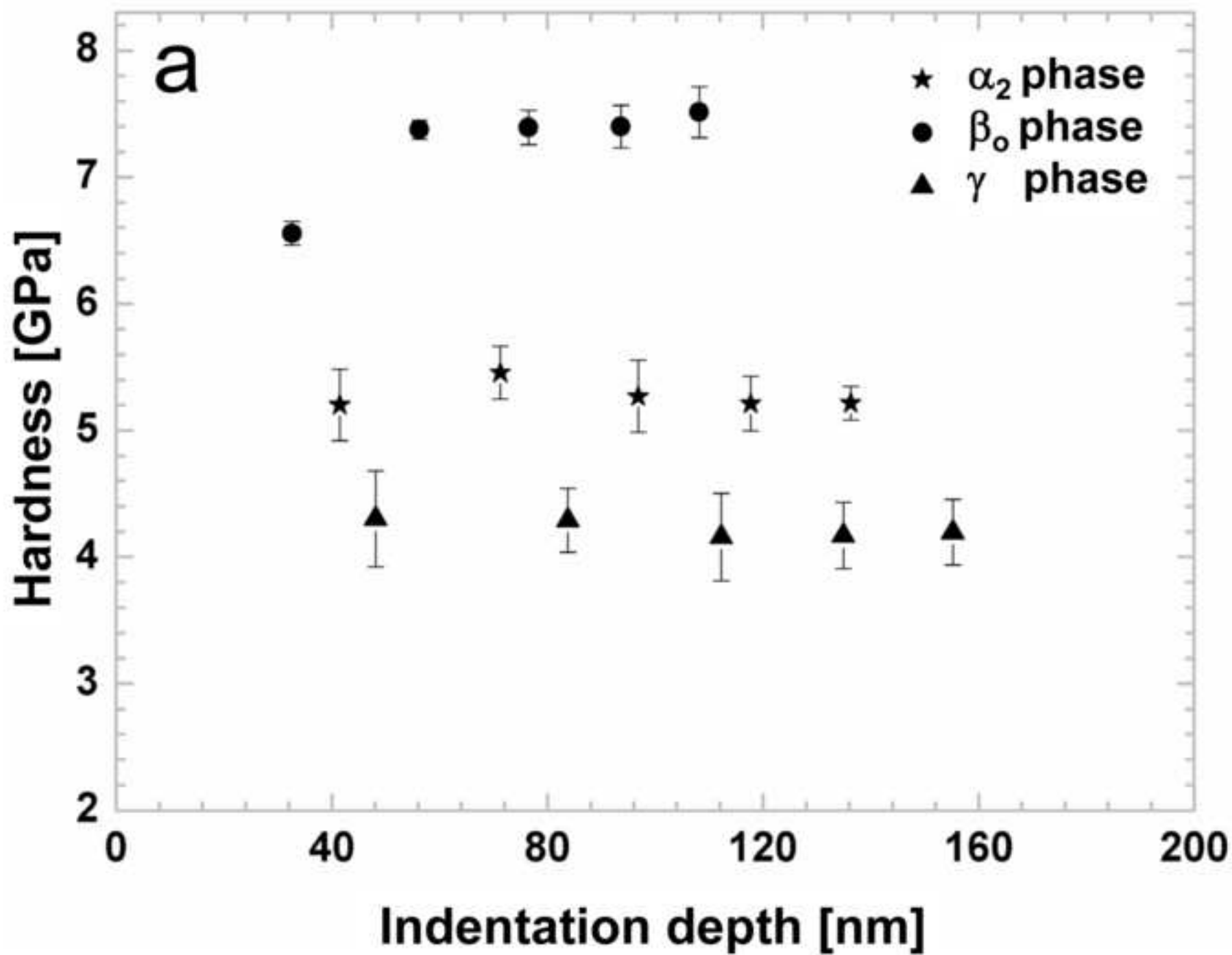
[Click here to download high resolution image](#)

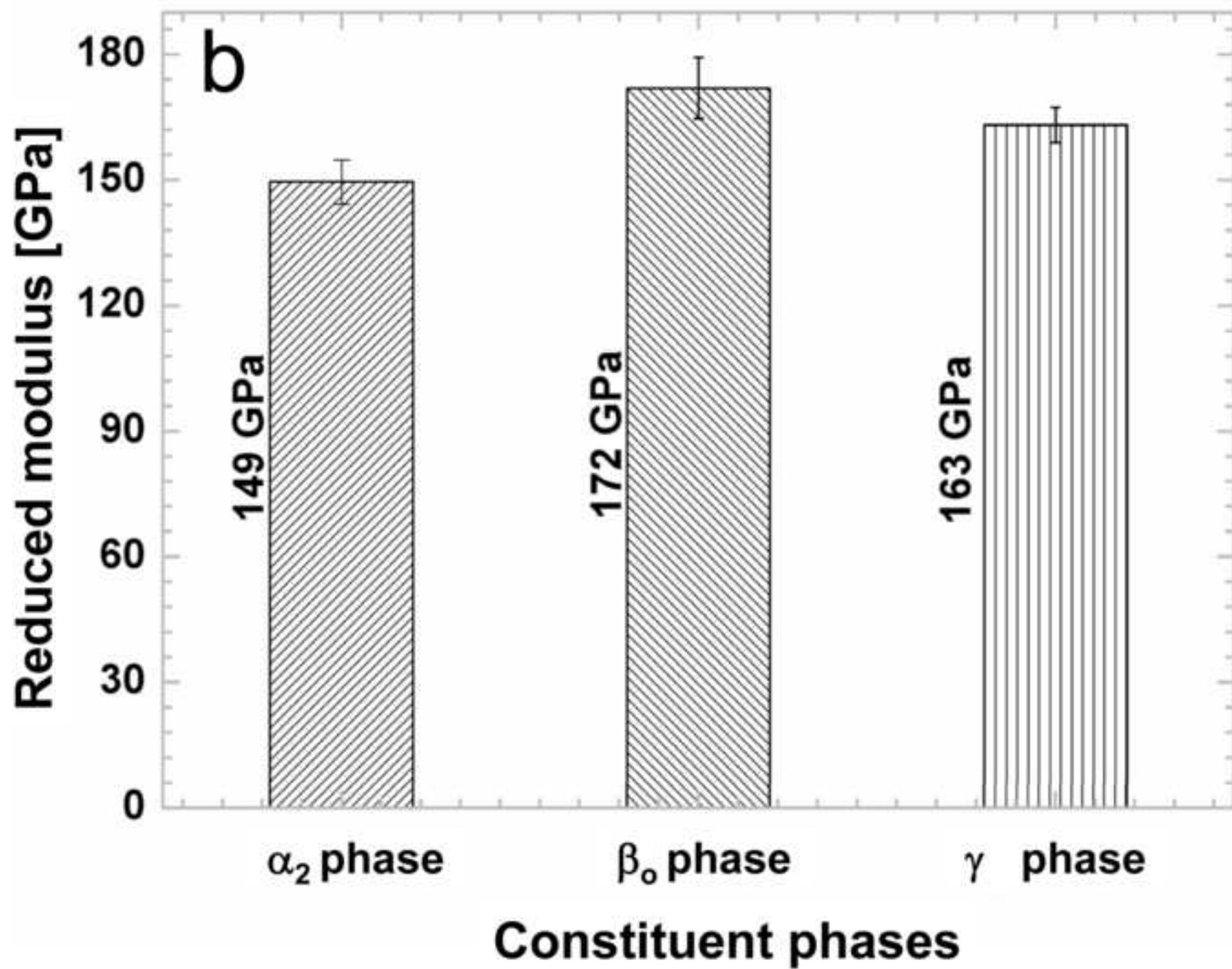


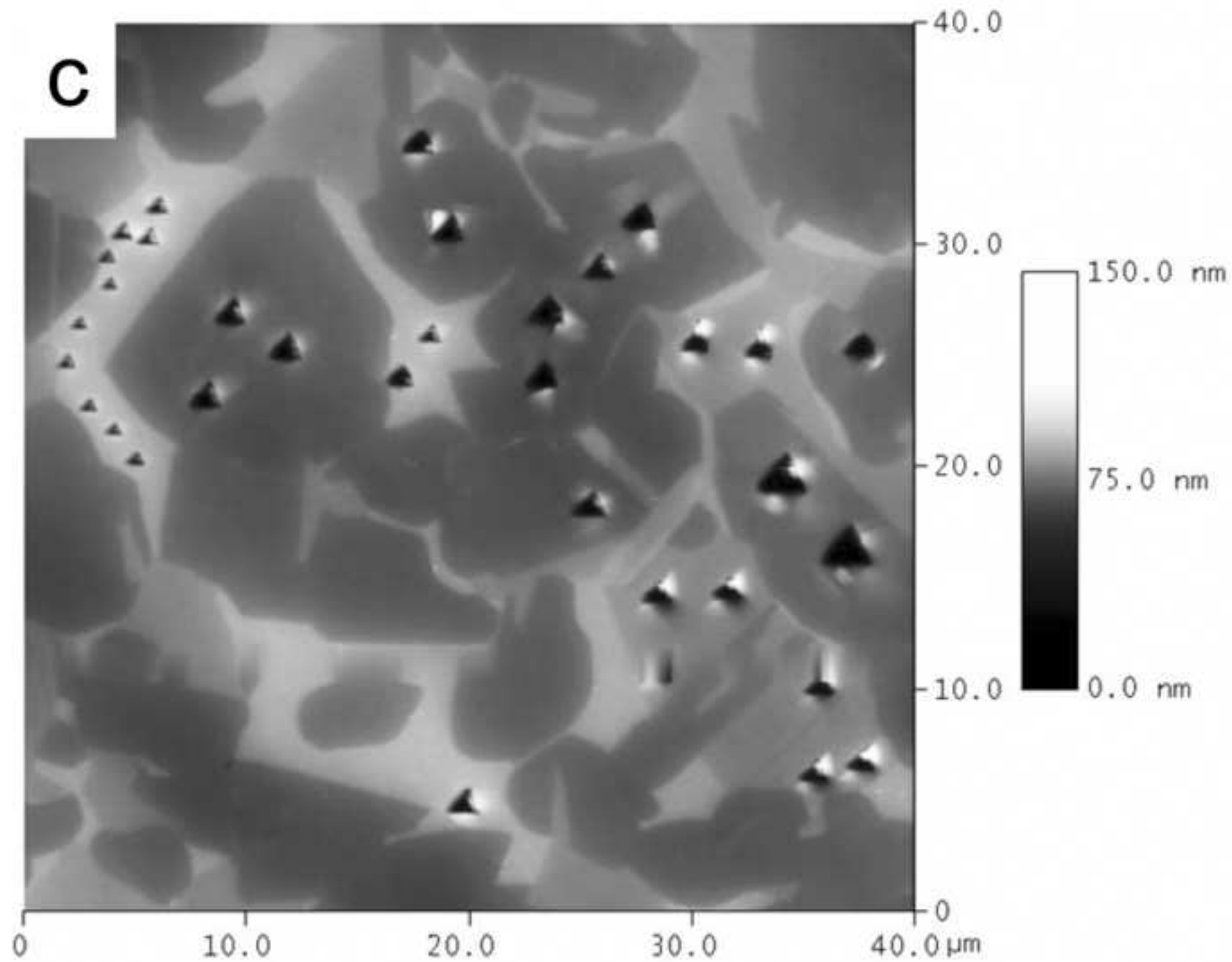


Figure(s)
[Click here to download high resolution image](#)

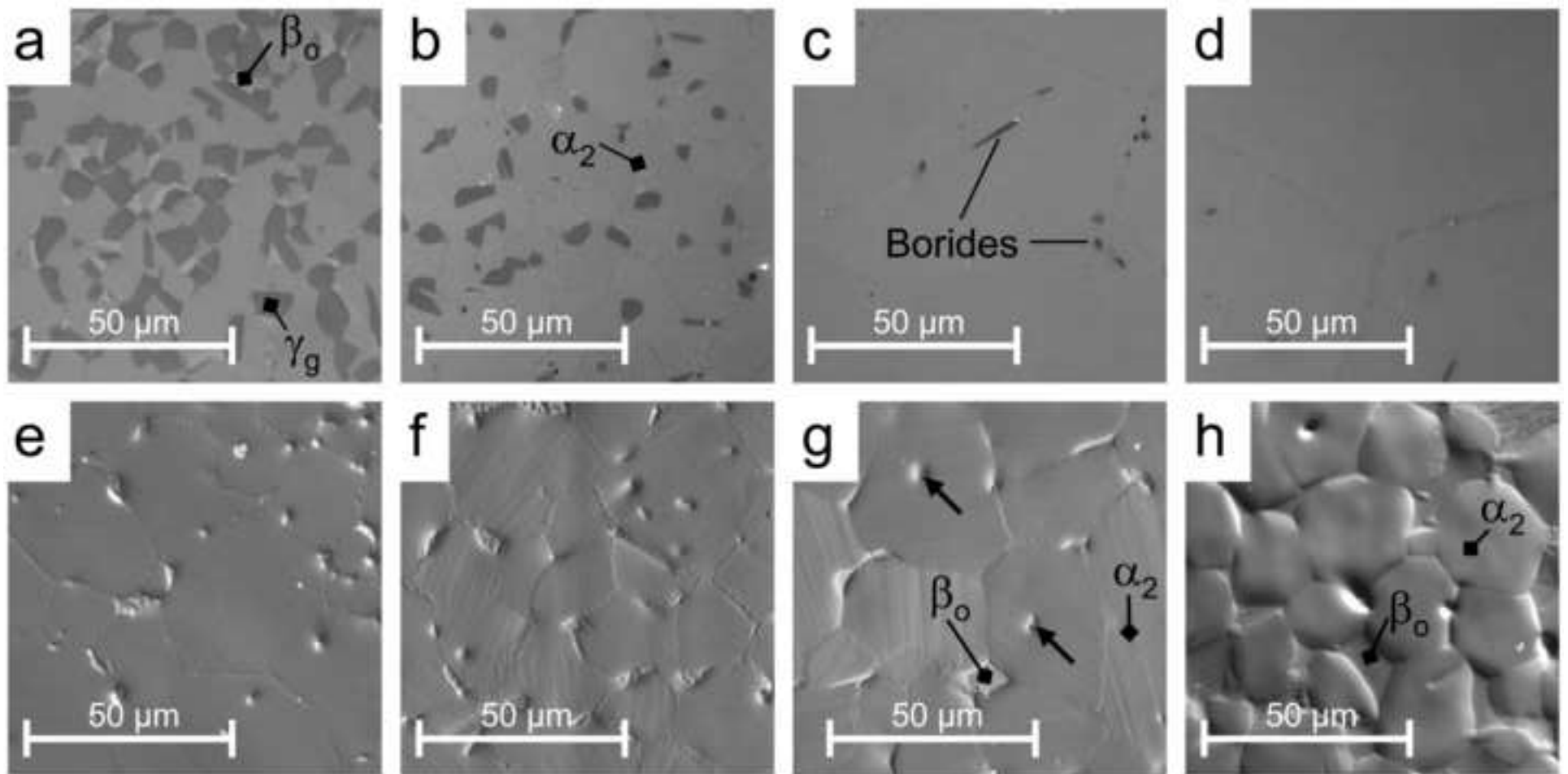


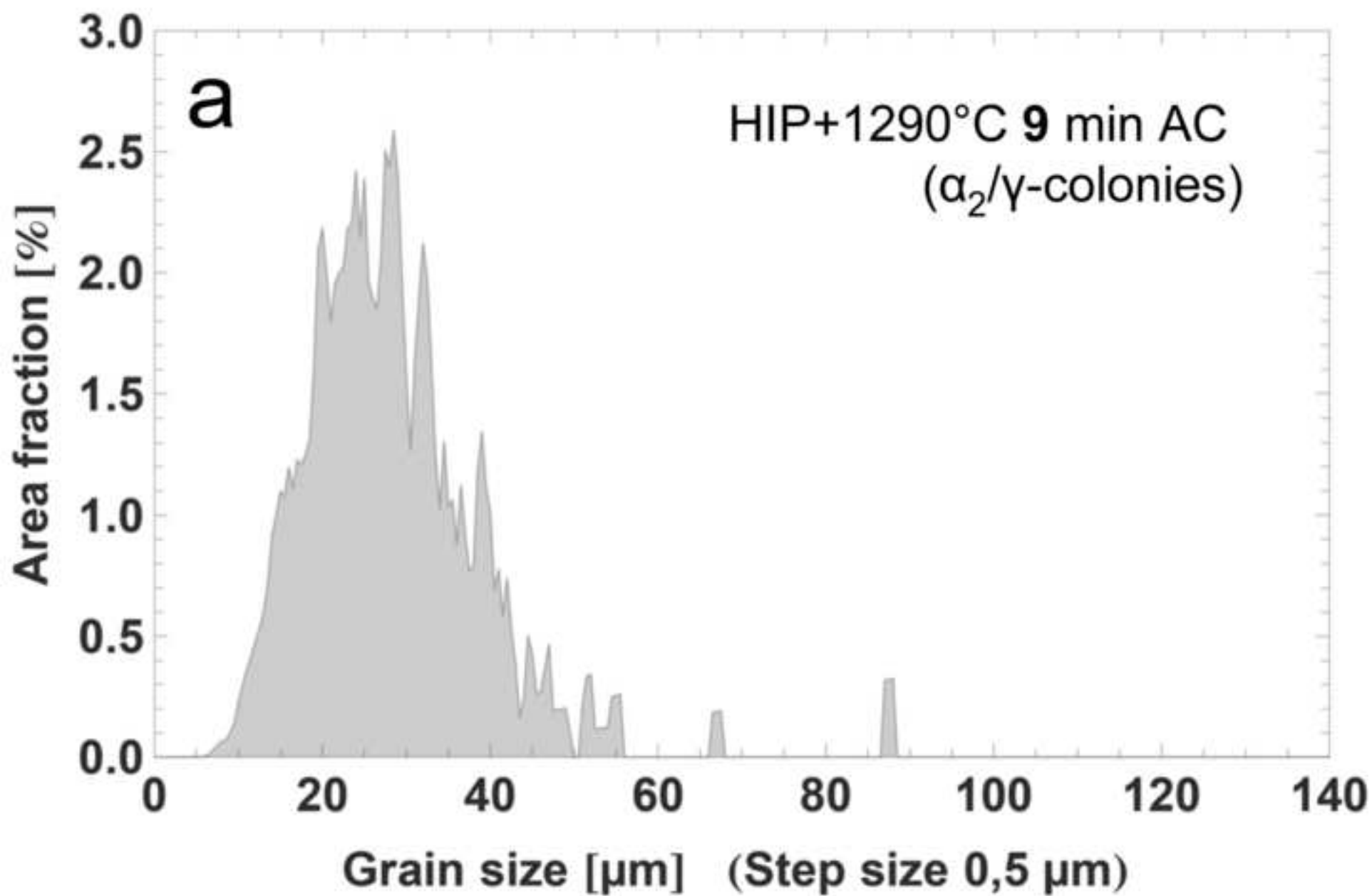


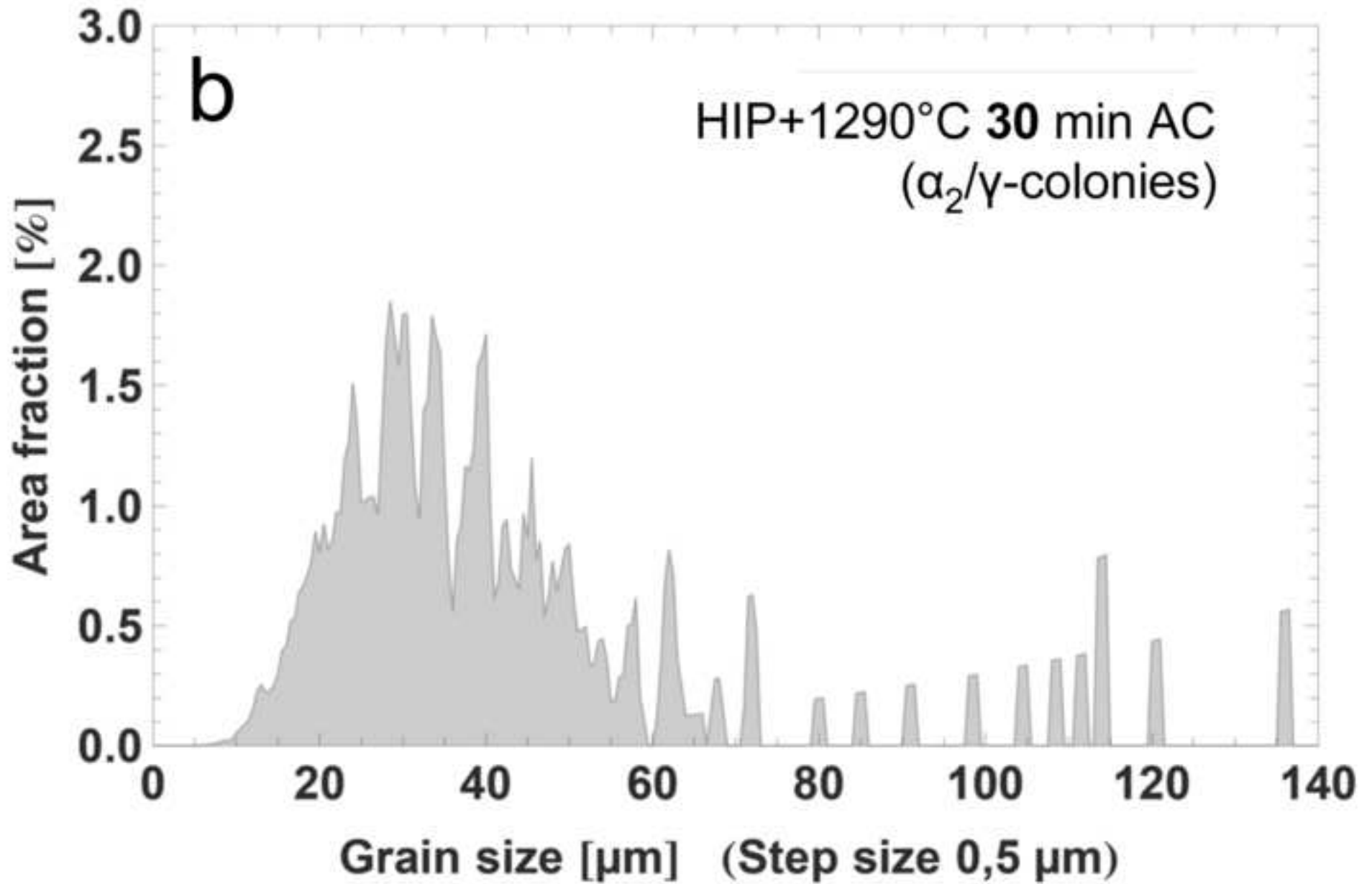




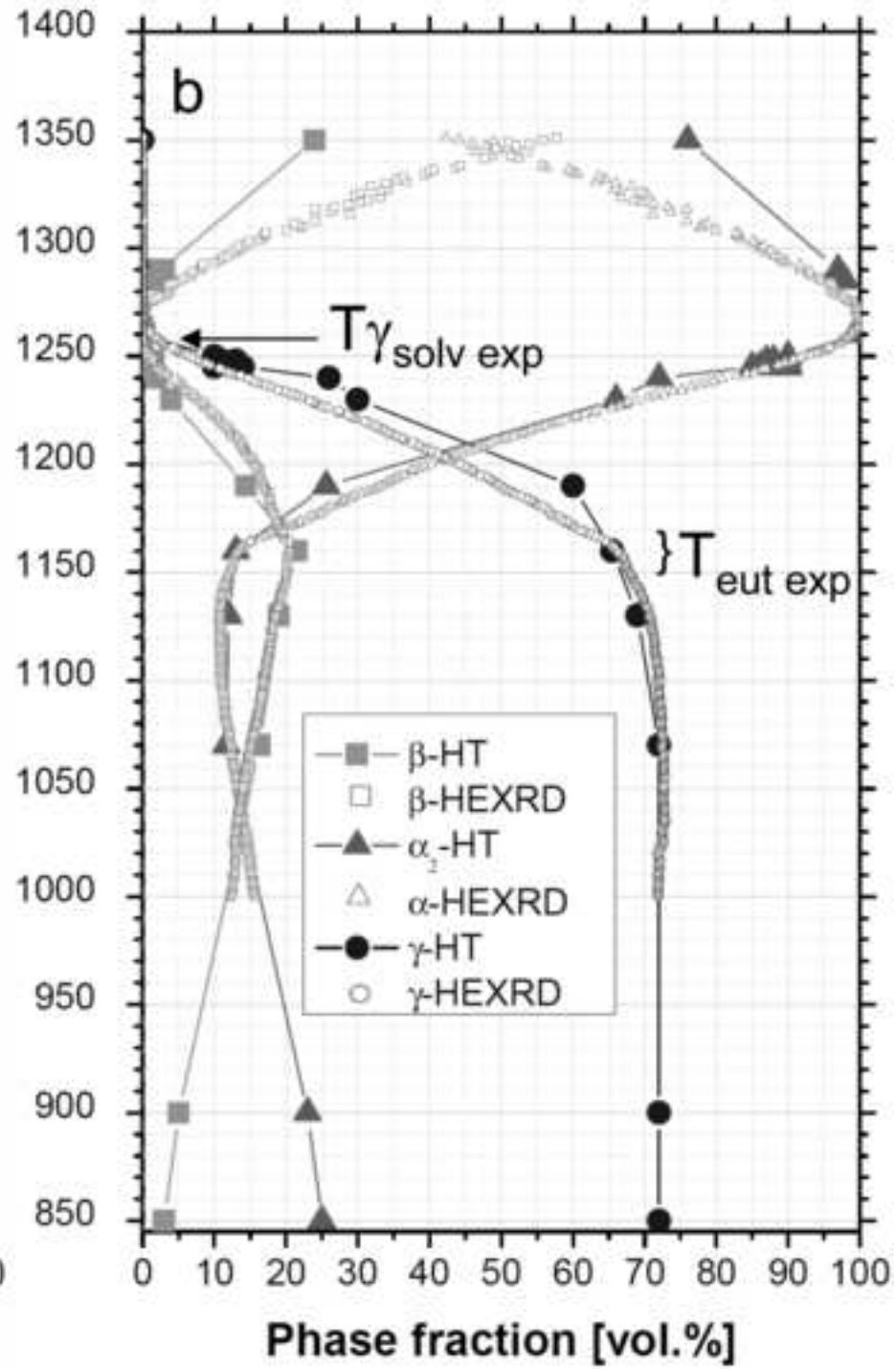
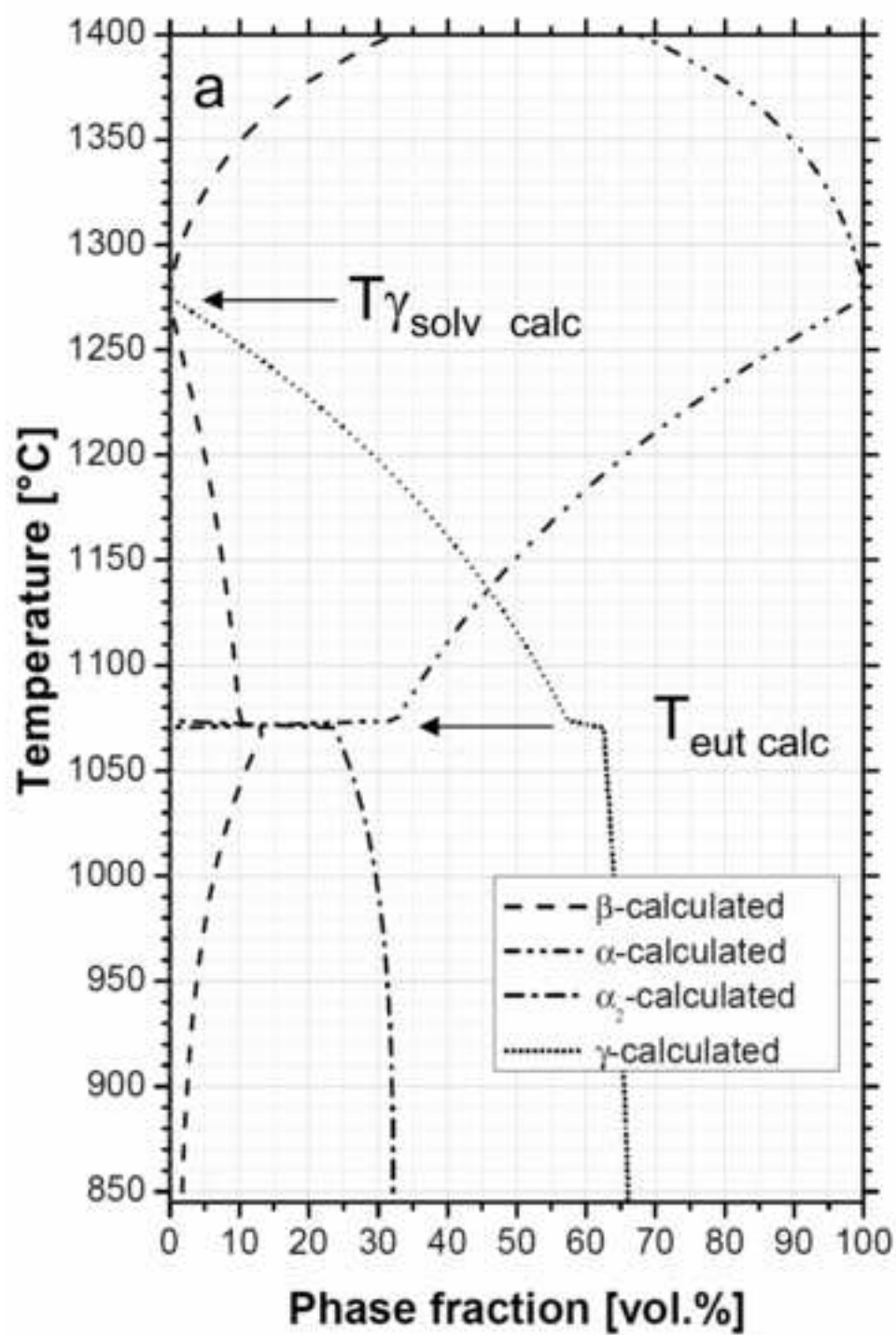
Figure(s)
[Click here to download high resolution image](#)

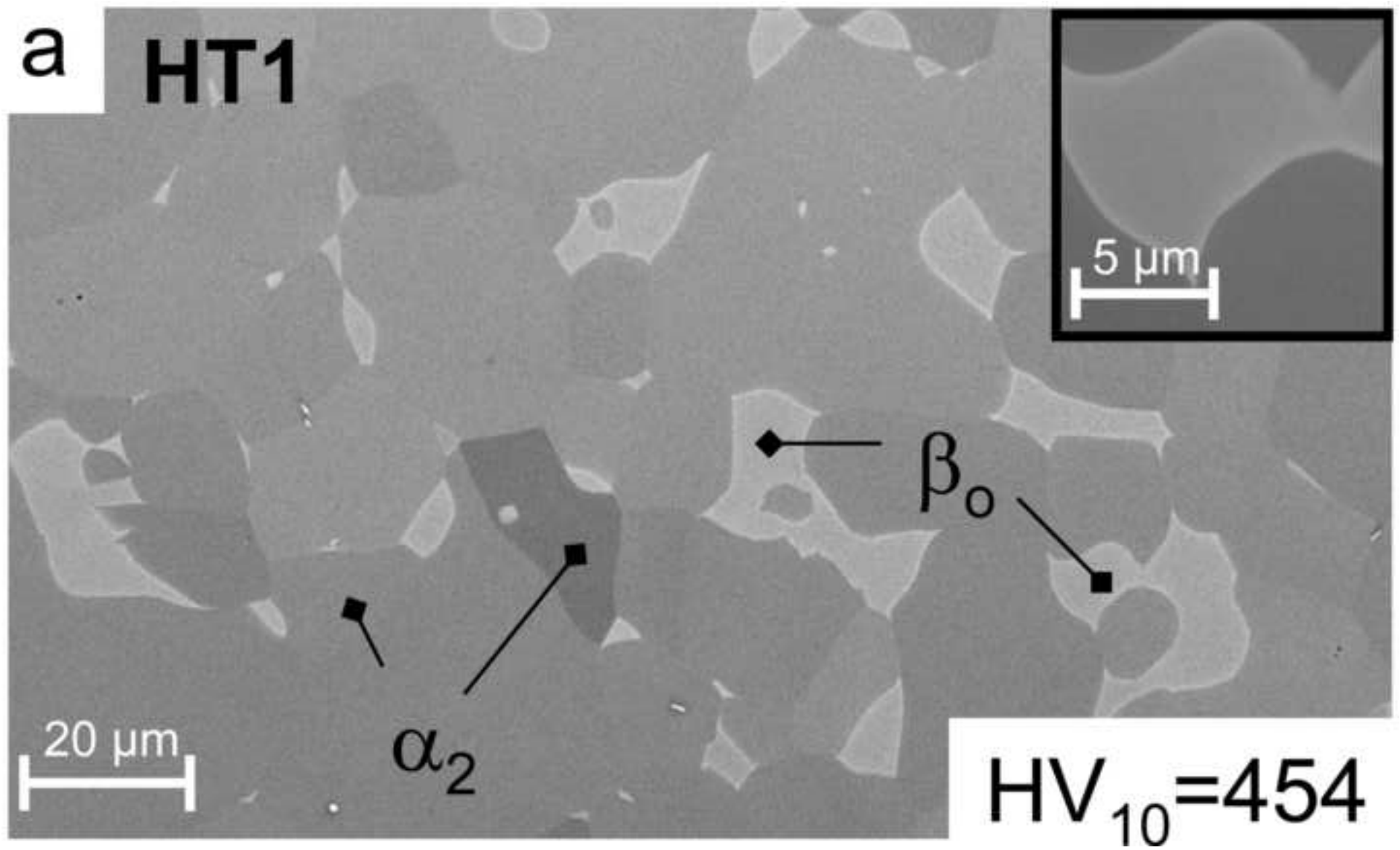


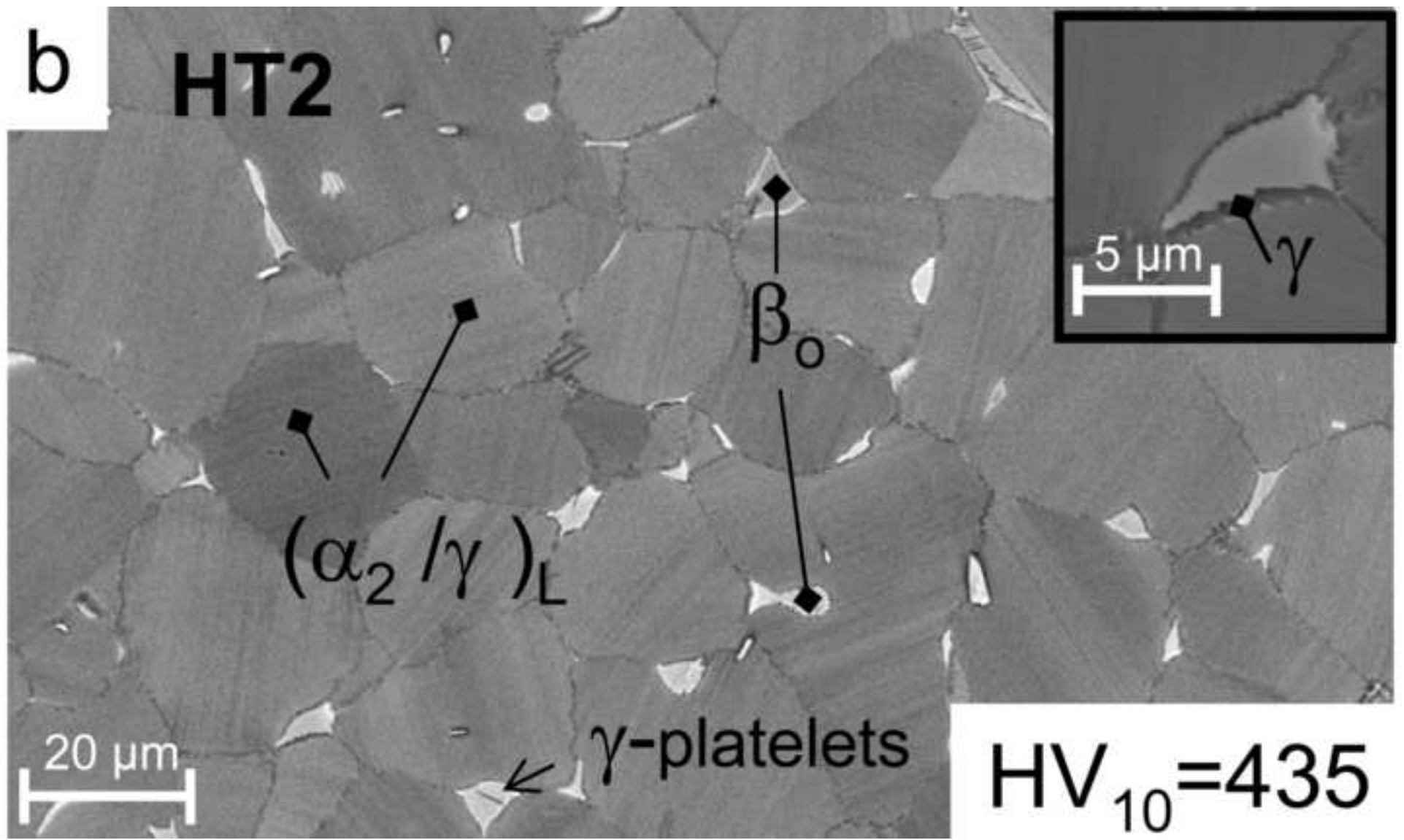


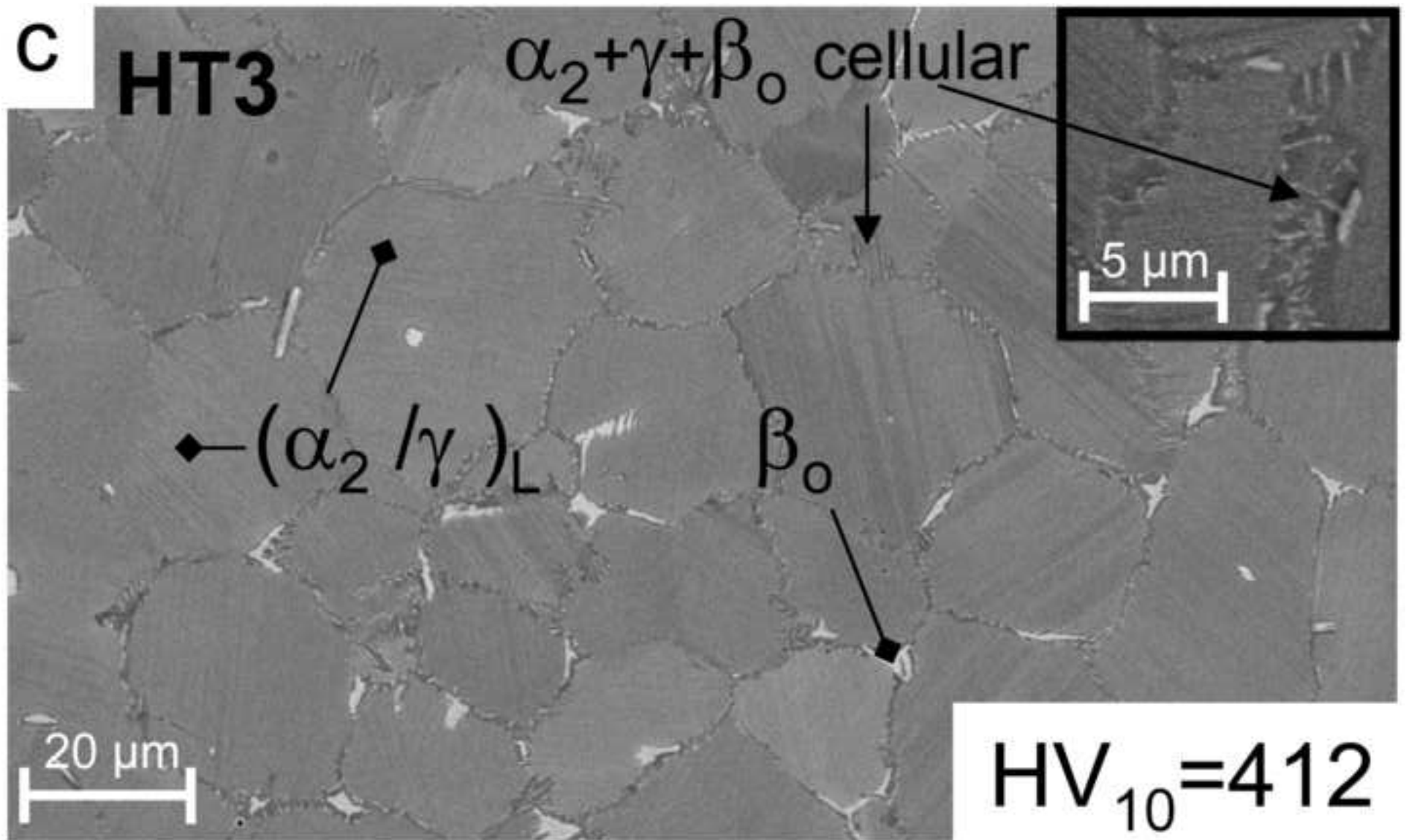


Figure(s)
[Click here to download high resolution image](#)



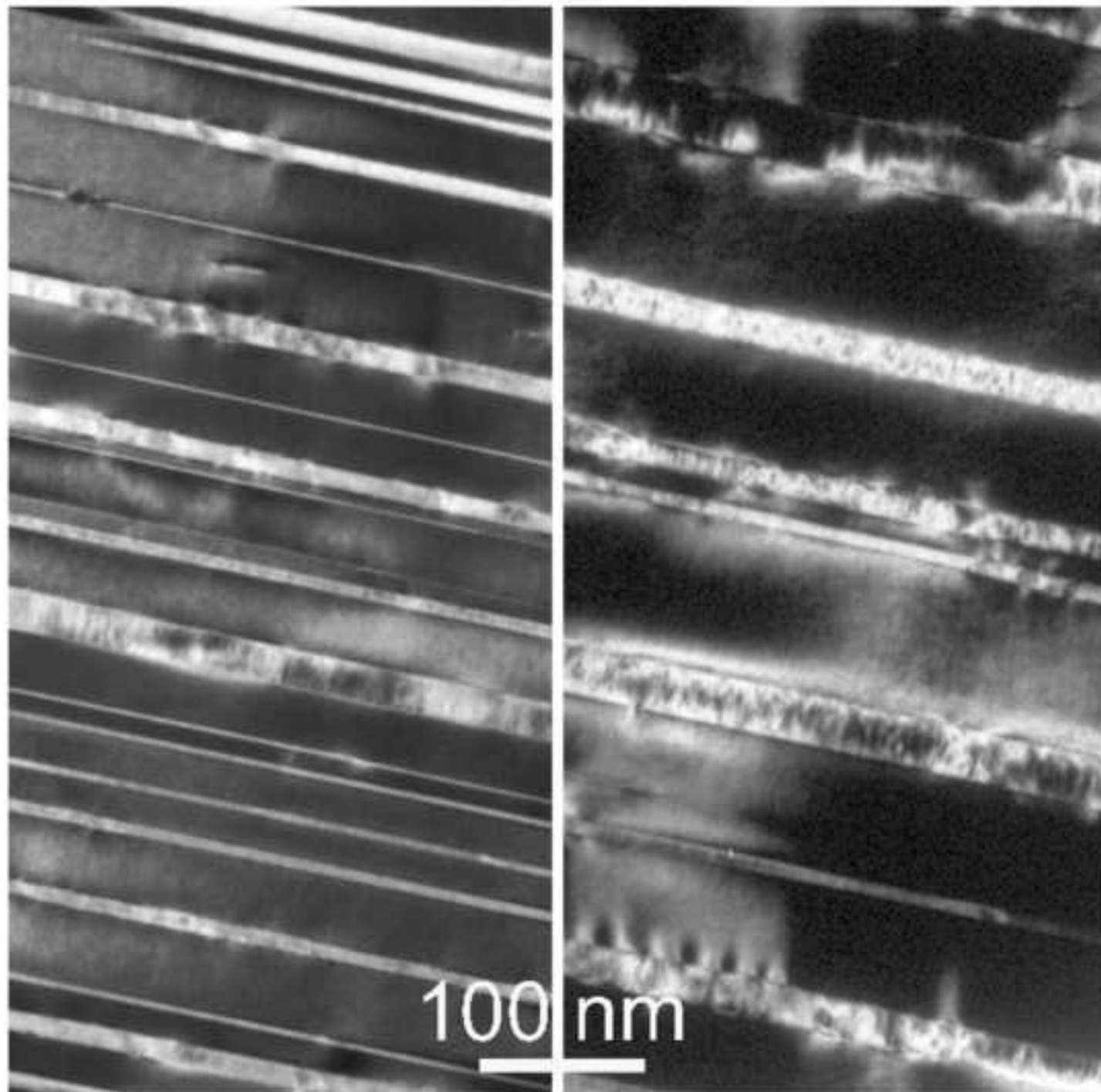






Figure(s)

[Click here to download high resolution image](#)



„Highlights of: Microstructure development and hardness of a powder metallurgical multi phase γ -TiAl based alloy“

> By means of two-step heat-treatments different fine grained nearly lamellar microstructures of a powder metallurgical processed TiAl TNM™ alloy were adjusted. > Nano-hardness measurements have been conducted on the three constituting phases α_2 , β_0 , and γ after hot-isostatic pressing. > The experimentally evaluated phase fractions as a function of temperature were compared with the results of a thermodynamical calculation. > The hardness modification during heat-treatment was studied by macro-hardness measurements.